Control Engineering Practice 97 (2020) 104307

Contents lists available at ScienceDirect

Control Engineering Practice

journal homepage: www.elsevier.com/locate/conengprac

Detection and diagnosis of oscillations in process control by fast adaptive chirp mode decomposition

Qiming Chen [a], Junghui Chen [b,*], Xun Lang [c], Lei Xie [a,*], Shan Lu [d], Hongye Su [a]

[a] State Key Laboratory of Industrial Control Technology, Zhejiang University, Hangzhou, 310027 Zhejiang, China
[b] Department of Chemical Engineering, Chung-Yuan Christian University, Chungli, Taoyuan 32023, Taiwan, ROC
[c] Department of Electronic Engineering, Information School, Yunnan University, Kunming 650091, China
[d] Shenzhen Polytechnic, Shenzhen 518055, China

ARTICLE INFO

Keywords:
Control performance monitoring
Fast adaptive chirp mode decomposition
Oscillation detection and diagnosis

ABSTRACT

Even though several algorithms have been proposed in the literature for oscillation detection and diagnosis, they can work reliably only for a specific type of oscillation and there is a lack of a common framework that accommodates the detection and diagnosis for various types of oscillations. To tackle this problem, an FACMD-based (fast adaptive chirp mode decomposition) detection and diagnosis framework is established in this study. It consists of two common oscillation detection indices and a novel strategy for diagnosing nonlinear and linear oscillations. Apart from detecting and diagnosing various single/multiple oscillations in single-input single-output (SISO) loop, FACMD can also distinguish the combination of linear or nonlinear oscillations and contribute to the root cause analysis for plant-wide oscillations. Finally, a series of simulations and industrial cases are used for testing. Compared with the existing work, the proposed methodology has better detection and diagnosis accuracy and a higher level of automation, especially in processing complex multiple oscillations.

1. Introduction

Oscillations have a detrimental effect on the control loop performance. They can cause plants to be run in sub-optimal conditions and may result in the waste of raw materials, increased energy consumption, and even compromised stability and safety. Therefore, oscillation detection and diagnosis is of crucial importance in maintaining the performance of control loops. Over the past decades, methods of oscillation detection and diagnosis have been developed rapidly. Fig. 1 briefly summarizes the development of the methods and this proposed method on oscillation detection and diagnosis. A brief overview is provided as follows.

1.1. Methods for oscillation detection and diagnosis

Iwashita (1992) firstly proposed a method for oscillation detection of a servo system. The first detection algorithm in control loops was proposed by Hägglund (1995). It was developed based on computing the regularity of large enough integral absolute errors (IAEs) between successive zero-crossings of the control errors. Later, Forsman and Stattin (1999) presented a modified method based on the regularity of upper and lower IAEs. In addition to those IAE-based methods, various auto-covariance function (ACF)-based methods were widely exploited to detect oscillations (Miao & Seborg, 1999) as the ACF of an oscillatory signal can filter out noise while reflecting the oscillatory property presented in the signal. However, all the above methods are only applicable to time series with single oscillations.

With respect to detecting multiple oscillations, this difficulty was initially overcome by means of bandpass filtering, in which the filter boundaries were selected from the inspection in the power spectral density (PSD) (Thornhill, Huang and Zhang, 2003). This technique can isolate components of different frequencies via band-pass filters, but its performance is affected by the selected frequency band. To tackle this issue, Naghoosi and Huang (2014a) proposed to identify the multiple oscillations directly by clustering the ACF peaks with similar amplitude and evaluate the regularity for each other. However, this method relies on restrictive assumptions that the oscillation signal should be stationary and its magnitude/frequency is not time-varying.

Once oscillations are detected, the next task is to diagnose the corresponding causes, which can be classified into three types, including external harmonic disturbances, poor control tuning, or nonlinearity. Generally, oscillations can be classified into linear oscillations and oscillations induced by nonlinearities. Nonlinear oscillations have a distinct property, which makes them distinguishable from the other types of oscillations (Naghoosi & Huang, 2014b). In addition to the main frequency oscillation, nonlinear oscillations have several harmonics with phase coupling. Therefore, the methods like surrogate data (Thornhill,

* Corresponding authors.
E-mail addresses: jason@wavenet.cycu.edu.tw (J. Chen), leix@iipc.zju.edu.cn (L. Xie).

https://doi.org/10.1016/j.conengprac.2020.104307
Received 14 September 2019; Received in revised form 21 December 2019; Accepted 20 January 2020
Available online 4 February 2020
0967-0661/© 2020 Elsevier Ltd. All rights reserved.

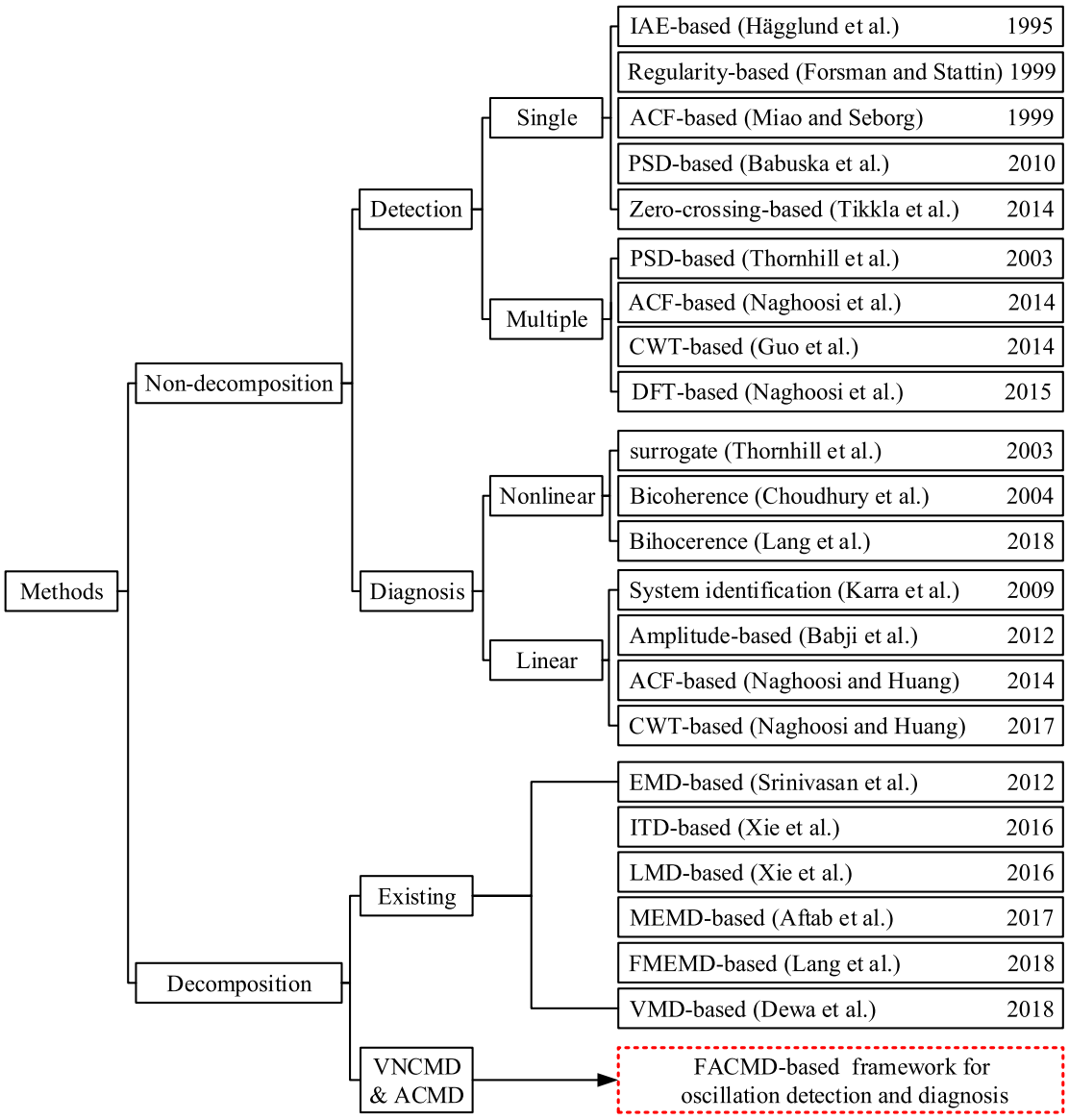

Fig. 1. A brief list of oscillation detection and diagnosis methods. FACMD is the proposed method in this paper; it is shown in the red dash box.

Cox and Paulonis, 2003), bihocerence (Lang et al., 2018), etc. are suitable for the detection and diagnosis of nonlinear oscillations. The other two types of linear oscillations, i.e., external harmonic disturbance, and oscillation induced by poor controller tuning are very similar to each other, and there is a lack of techniques to distinguish them (Naghoosi & Huang, 2014b). Karra and Karim (2009) first proposed a solution using a system identification approach to distinguish between external disturbance and oscillations caused by controller tuning. Then, Babji, Nallasivam, and Rengaswamy (2012) proposed a method based on the assumption that oscillation caused by poor tuning has a higher amplitude than the external harmonic disturbance. Recently, Naghoosi and Huang (2014b) used different peaks between ACF and signal-to-noise (SNR) to distinguish linear oscillations of process variables (PVs), which is the most significant progress. However, this approach can only deal with a single oscillation. Then they tried to detect and characterize the multiple oscillations by wavelet transform (Naghoosi & Huang, 2017). This method may be useful, but it is also limited by the shortcomings of wavelet transform in essence, such as the choice of mother wavelet and scale. This work (Naghoosi & Huang, 2017) is the most advanced methodology so far, and we will compare and discuss our method with it in detail later.

1.2. Motivations and contributions

With the development of signal decomposition, many related techniques have been introduced to oscillation detection and diagnosis. They have greatly improved the level of control performance monitoring. They become hot research topics, such as EMD-based (empirical mode decomposition) (Srinivasan, Rengaswamy, & Miller, 2007), ITD-based (intrinsic time-scale decomposition) (Guo, Xie, Ye, & Horch, 2014), LMD-based (local mean decomposition) (Xie, Lang, Chen, Horch, & Su, 2016), MEMD-based (Aftab, Hovd, & Sivalingam, 2017, 2018a), FMEMD-based (fast multivariate EMD) (Lang et al., 2018), VMD-based (variational mode decomposition) (Dewa, Wardana, & Hawibowo, 2018). They suppose that the signal components satisfy strict separation conditions in the time-frequency domain, so they cannot fully separate those close or overlapped signal components. In addition, all the above methods cannot handle mode-mixing, poor noise robustness, and low-frequency resolutions. In this work, a powerful signal processing tool called variational nonlinear chirp mode decomposition (VNCMD) was introduced (Chen, Dong, Peng, Zhang, & Meng, 2017). It was derived by solving an optimal demodulation problem, so it is capable of accurately estimating the instantaneous frequencies (IFs) and instantaneous amplitudes (IAs) of signals with very close or even

crossed modes. However, both the mode number and the bandwidth parameter should be specified in advance. Actually, they need to adjust themselves according to different stages of the optimization. To tackle these issues, Chen et al. (2019) proposed an adaptive chirp mode decomposition (ACMD), which was a tractable version of VNCMD, and showed better resolution than current time-frequency distributions. ACMD has been successfully applied to fault diagnosis of rotor-stator systems (Chen et al., 2019), but its application in industrial control systems has not been reported.

Although past research focused on oscillation detection and diagnosis, there is still no common framework that accommodates the detection and diagnosis of various types of oscillations (Ullah, Das, Parmar, Rengaswamy, & Srinivasan, 2019). Thus, the main goals of this work will cover:

(1) A detailed literature survey is conducted and a discussion of drawbacks of various methods for oscillation detection and diagnosis is highlighted.
(2) A fast ACMD (FACMD) algorithm is developed by modifying the convergence criterion of the vanilla ACMD using the correlation relationships and the energy ratio. It is expected to perform more efficiently than the vanilla ACMD.
(3) An integrated framework that addresses the challenges in oscillation detection and diagnosis is established based on FACMD. The FACMD-based framework includes (i) oscillation detection, (ii) a novel nonlinear oscillation diagnosis algorithm, and (iii) discrimination of linear oscillations. The framework can automatically detect and diagnose various linear and nonlinear oscillations without prior knowledge.
(4) Compared with the existing works (Aftab et al., 2017; Naghoosi & Huang, 2014b, 2017), the proposed methodology not only can distinguish the combination of different types of oscillations but also has better accuracy of detection and diagnosis and a higher level of automation, especially for complex multiple oscillations.

The integrated framework is detailed in the following sections. Section 2 provides an overview of VNCMD and ACMD, followed by the proposed FACMD elaborately. Sections 3 and 4 describe the detailed algorithm of oscillation detection and diagnosis, respectively. The simulation and industrial cases are studied in Section 5, followed by conclusions.

2. From VNCMD and ACMD to FACMD

2.1. VNCMD

VNCMD (Chen et al., 2017) is developed based on the fact that a wideband nonlinear chirp signal can be transformed into a narrowed-band signal using demodulation techniques. This decomposition method is a generation of VMD (Dragomiretskiy & Zosso, 2013). It assumes that a non-stationary signal $x(t)$ is composed of K AM-FM (amplitude-modulated and frequency-modulated) functions and expressed as

$$x(t)=\sum_{m=1}^{K}x_m(t)=\sum_{m=1}^{K}a_m(t)\cos\left(2\pi\int_0^t f_m(s)\,ds+\phi_m\right)+n(t) \tag{1}$$

where $x(t)$ is a superposition of K modes $x_m(t)$ for $m=1,2,\ldots,K$; $a_m(t)>0$, $f_m(t)>0$ and ϕ_m denote the instantaneous amplitude (IA), the instantaneous frequency (IF) and the initial phase of the mth mode, respectively. Generally, IA and IF are assumed to be smooth functions. They vary more slowly than their phase function, i.e. $|a_m'(t)|, |f_m'(t)| \ll f_m(t)$. Based on the demodulation techniques, Eq. (1) can be rewritten as the de-chirped form as

$$x(t)=\sum_{m=1}^{K}\alpha_m(t)\cos\left(2\pi\int_0^t \widetilde{f}_m(s)\,ds\right)+\beta_m(t)\sin\left(2\pi\int_0^t \widetilde{f}_m(s)\,ds\right) \tag{2}$$

with

$$\alpha_m(t)=a_m(t)\cos\left(2\pi\int_0^t\left(f_m(s)-\widetilde{f}_m(s)\right)ds+\phi_m\right), \tag{3}$$

$$\beta_m(t)=-a_m(t)\sin\left(2\pi\int_0^t\left(f_m(s)-\widetilde{f}_m(s)\right)ds+\phi_m\right) \tag{4}$$

where $\alpha_m(t)$ and $\beta_m(t)$ are two de-chirped (demodulated) signals which can recover IA as $a_m(t)=\sqrt{\alpha_m^2(t)+\beta_m^2(t)}$; $\widetilde{f}_m(s)$ is the estimated frequency function of the two demodulation operators $\cos\left(2\pi\int_0^t\widetilde{f}_m(s)\,ds\right)$ and $\sin\left(2\pi\int_0^t\widetilde{f}_m(s)\,ds\right)$. If $f_m(t)=\widetilde{f}_m(t)$ ideally, the demodulated signals $\alpha_m(t)$ and $\beta_m(t)$ will purely be AM (amplitude-modulated) signals which are slowly varying baseband signals with narrowest bandwidths. Therefore, VNCMD estimates the signal modes by minimizing the bandwidths of the demodulated signals as

$$\begin{aligned}&\min_{\{\alpha_m(t)\},\{\beta_m(t)\},\left\{\widetilde{f}_m(t)\right\}}\left\{\sum_{m=1}^{K}\left\|\alpha_m''(t)\right\|_2^2+\left\|\beta_m''(t)\right\|_2^2\right\}\\ &s.t.\quad x(t)=\sum_{m=1}^{K}a_m(t)\cos\left(2\pi\int_0^t f_m(s)\,ds+\phi_m\right)\end{aligned} \tag{5}$$

where $\|\cdot\|_2$ stands for the l_2 norm. This constrained optimization problem can be solved by the augmented Lagrange multiplier method (Chen et al., 2017).

2.2. ACMD

Although VNCMD has remarkable performance in signal decomposition, one of its major limitations is that the number of modes K and the corresponding IFs should be provided in advance. However, it is difficult to know all the mentioned information in real environments. To tackle the issue, Chen, Yang, Peng, Dong et al. (2019) proposed a tractable version of VNCMD, termed as adaptive chirp mode decomposition (ACMD). The main parts of ACMD consist of a recursive mode extraction framework, an adaptive bandwidth updating rule, and an IF initialization scheme based on Hilbert transform. Specifically, for the mth mode, ACMD solves the following problem

$$\min_{\{\alpha_m(t)\},\{\beta_m(t)\},\left\{\widetilde{f}_m(t)\right\}}\left\|\alpha_m''\right\|_2^2+\left\|\beta_m''\right\|_2^2+\tau\left\|x(t)-x_m(t)\right\|_2^2 \tag{6}$$

with

$$x_m(t)=\alpha_m(t)\cos\left(2\pi\int_0^t\widetilde{f}_m(s)\,ds\right)+\beta_m(t)\sin\left(2\pi\int_0^t\widetilde{f}_m(s)\,ds\right) \tag{7}$$

where the l_2 norm of the second derivative ($\left\|\alpha_m''\right\|_2^2+\left\|\beta_m''\right\|_2^2$) imposes smoothness constraints on $\alpha_m(t)$ and $\beta_m(t)$, just like Eq. (5); τ is a weighting factor of the energy of the residual.

Assume that the time series are sampled at $t=t_0,t_1,\ldots,t_{N-1}$. The discrete version of Eq. (6) can be obtained as

$$J_\tau(\mathbf{y}_m,\mathbf{f}_m)=\left\|\mathbf{\Phi}\mathbf{y}_m\right\|_2^2+\tau\left\|\mathbf{x}-\mathbf{K}_m\mathbf{y}_m\right\|_2^2 \tag{8}$$

where $\mathbf{x}=\left[x(t_0),\ldots,x(t_{N-1})\right]^T$, $\mathbf{f}_m=\left[f_m(t_0),\ldots,f_m(t_{N-1})\right]^T$; $\mathbf{y}_m=\left[\alpha_m^T\,\beta_m^T\right]^T$ with $\alpha_m=\left[\alpha_m(t_0),\ldots,\alpha_m(t_{N-1})\right]^T$, $\beta_m=\left[\beta_m(t_0),\ldots,\beta_m(t_{N-1})\right]^T$; the kernel matrix is $\mathbf{K}_m=\left[\mathbf{C}_m\,\mathbf{S}_m\right]$ with $\mathbf{C}_m=diag\left[\cos\left(\varphi_m(t_0)\right),\ldots,\cos\left(\varphi_m(t_{N-1})\right)\right]$, $\mathbf{S}_m=diag\left[\sin\left(\varphi_m(t_0)\right),\ldots,\sin\left(\varphi_m(t_{N-1})\right)\right]$, where $\varphi_m(t)=2\pi\int_0^t\widetilde{f}_m(s)\,ds$; $\mathbf{\Phi}=\begin{bmatrix}\mathbf{D}&\mathbf{0}\\ \mathbf{0}&\mathbf{D}\end{bmatrix}$, in which $\mathbf{0}$ is a zero matrix and $\mathbf{D}$ is a second-order difference matrix.

$$\mathbf{D}=\begin{bmatrix}-1&1&0&\cdots&0\\ 1&-2&1&\cdots&0\\ \vdots&\ddots&\ddots&\ddots&\vdots\\ 0&\cdots&1&-2&1\\ 0&\cdots&0&1&-1\end{bmatrix}_{(N-2)\times N}.$$

Motivated by the matching pursuit-like method, ACMD uses a greedy algorithm to extract the sub-signals one by one and the corresponding

procedures are shown in Algorithm 1.[1] For more details, refer to Chen, Yang, Peng, Dong et al. (2019). Although ACMD using a recursive mode extraction scheme is the latest development in the field of signal decomposition with some promising advantages, it is prone to the over-decomposition problem and it cannot distinguish white noise (the normal working condition) from fault signals. In this paper, these limitations are solved and the proposed scheme is detailed in the following sections.

Algorithm 1: ACMD

Input: $\mathbf{x}$; parameter μ, τ^1; stopping threshold δ, ε

Output: $\{\mathbf{x}_m\}_{m=1,2,\ldots}$, $\{\mathbf{f}_m\}_{m=1,2,\ldots}$

1: set $m=1$, $r_1 = x$

2: **while** $\|\mathbf{r}_m\|_2^2 / \|\mathbf{x}\|_2^2 > \delta$ **do**

3: $n=0$, initialize IF $f_m^1(t)$ and $\mathbf{W}_m^1$

4: **while** $\left\|x_m^n - x_m^{n-1}\right\|_2^2 / \left\|x_m^{n-1}\right\|_2^2 > \varepsilon$ **do**

5: $n = n+1$

6: $\mathbf{y}_m^n = \left(\frac{1}{\tau^1}\mathbf{\Phi}^T\mathbf{\Phi} + \left(\mathbf{W}_m^n\right)^T\mathbf{W}_m^n\right)^{-1}\left(\mathbf{W}_m^n\right)^T\mathbf{r}_m$

7: $\mathbf{x}_m^n = \mathbf{W}_m^n\mathbf{y}_m^n$

8: $\Delta\tilde{f}_m^n(t) = \frac{\beta_m^n(t)\cdot\left(\alpha_m^n(t)\right)' - \alpha_m^n(t)\cdot\left(\beta_m^n(t)\right)'}{2\pi\left(\alpha_m^n(t)\right)^2 + 2\pi\left(\beta_m^n(t)\right)^2}$

9: $\mathbf{f}_m^{n+1} = \mathbf{f}_m^n + \left(\mathbf{I} + \frac{1}{\mu}\mathbf{D}^T\mathbf{D}\right)^{-1}\Delta\tilde{\mathbf{f}}_m^n$

10: Update kernel matrix $\mathbf{W}_m^{n+1}$

11: $\tau^{n+1} = \frac{\tau^n\left(\mathbf{x}_m^n\right)^T\mathbf{x}_m^n}{\left(\mathbf{x}_m^n\right)^T\mathbf{r}_m}$

12: **end while**

13: $\mathbf{x}_m = \mathbf{x}_m^n$, $\mathbf{f}_m = \mathbf{f}_m^{n+1}$, and $\mathbf{r}_{m+1} = \mathbf{x} - \mathbf{x}_m$

14: $m = m+1$

15: **end while**

2.3. Fast ACMD

2.3.1. Two improvements of the vanilla ACMD

The vanilla ACMD has two evident shortcomings. Firstly, its mode number is learned by assessing the energy of the residual signal (Step 2 in Algorithm 1), which is highly correlated with the signal noise level. However, estimating noise levels in real signals is a challenging task, so the adaptability of the vanilla ACMD is limited. To improve the accuracy, the relationship between the extracted modes and the original signal is used as the stopping criterion for the outer loop, rather than the energy of the residual signal. In this way, the mode number can be determined by the signal itself based on different stages of the optimization. The correlation coefficient is an ideal index to measure such a relationship given as

$$\rho_m = \frac{cov\left(x_m, x\right)}{std\left(x\right) std\left(x_m\right)}, \quad m = 1, 2, 3, \ldots, K \tag{9}$$

where $cov(\cdot)$ and $std(\cdot)$ symbolize the covariance and the standard deviation, respectively. The normalized correlation coefficient can be calculated by

$$\lambda_m = \frac{\rho_m}{\max\left\{\rho_1, \rho_2, \ldots, \rho_K\right\}}, \quad m = 1, 2, 3, \ldots, K \tag{10}$$

However, the above original definition of the normalized correlation coefficient cannot be directly applied to ACMD as the mode number K is unknown during the iteration. Therefore, updating λ_j is proposed, i.e.

$$\lambda_j = \frac{\rho_j}{\max\left\{\rho_1, \rho_2, \ldots, \rho_m\right\}}, \quad j = 1, 2, 3, \ldots \tag{11}$$

Algorithm 2: Fast ACMD

Input: $\mathbf{x}$; parameter μ, τ^1; stopping threshold $\delta, \varepsilon, \mu_\lambda$, μ_n

Output: $\{\mathbf{x}_m\}_{m=1,2,\ldots}$, $\{\mathbf{f}_m\}_{m=1,2,\ldots}$

1: set $m=1$, $\mathbf{r}_1 = \mathbf{x}$, $\lambda_1 = 1$, $\rho_{\max} = 0$, $ER_m = \|\mathbf{r}_m\|_2^2 / \|\mathbf{x}\|_2^2$

2: **while** $m < M_{\max}{}^2$ **do**

3: $n=0$, initialize $f_m^1(t)$, $\mathbf{W}_m^1$

4: The same as step 4 to 12 in the Algorithm 1 (ACMD)

5: $\mathbf{x}_m = \mathbf{x}_m^n$, $\mathbf{f}_m = \mathbf{f}_m^{n+1}$, $\rho_{new} = \rho_m$

6: **if** $\rho_{new} > \rho_{\max}$ **then** $\rho_{\max} = \rho_{new}$ **end if**

7: $\lambda_{1:m} = \rho_{1:m} / \rho_{\max}$

8: **if** $\lambda_m < \mu_\lambda$ **then** break **end if**

9: $\mathbf{r}_{m+1} = \mathbf{x} - \mathbf{x}_m$, $m = m+1$, $ER_m = \|\mathbf{r}_m\|_2^2 / \|\mathbf{x}\|_2^2$

10: **if** $ER_{1:3} > \mu_n$ **then** $\{\mathbf{x}_m\}_{m=1} = \mathbf{x}$, $\{\mathbf{f}_m\}_{m=1} = \mathbf{f}$ **end if**

11: **end while**

where m is the number of currently extracted modes. This novel modified procedure is described in detail from Step 6 till Step 8 of Algorithm 2. During those steps, the threshold $\mu_\lambda = 0.15$ is recommended and the selection of the threshold is discussed in Section 3.2.

Secondly, as the filter bank property of the vanilla ACMD, in essence, resembles that of the VMD (Dragomiretskiy & Zosso, 2013), the vanilla ACMD will decompose white noise into too many similar AM-FM modes, which means this method cannot distinguish noise from oscillation signals. However, in a real industrial control system, normal process outputs are often contaminated with noise. Thus it is necessary to improve the vanilla ACMD and make it effectively extract normal outputs from various signals; i.e. normal and oscillating loops are separated first. As the oscillation of the normal signal is mainly caused by noise, the rest of modes obtained by ACMD have almost equal energy and the energy ratio (ER) of each corresponding mode to the total energy is very small when the normal signal is extracted. Therefore, if

$$ER_m = \|\mathbf{r}_m\|_2^2 / \|\mathbf{x}\|_2^2 > \mu_n, m = 1, 2, 3 \tag{12}$$

the signal is regarded to be sampled from a normal case, where $\mu_n = 0.9$ is recommended. The discussion on the choice of the threshold is given in Section 3.2.

The above two improvements are summarized in Algorithm 2, which is termed as the fast ACMD (FACMD), as they can significantly speed up the vanilla ACMD by reducing the number of outer loops. The corresponding advantages and efficiency of FACMD are demonstrated as follows.

2.3.2. Comparison study

Two cases are used to demonstrate the merits of the proposed FACMD.

Case 1: A synthetic square wave signal (Eq. (13)) is written as

$$x(t) = \frac{4}{\pi}\sin(2\pi\times 10t) + \frac{4}{3\pi}\sin(2\pi\times 30t) + \frac{4}{5\pi}\sin(2\pi\times 50t) + \eta(t) \tag{13}$$

where $\eta(t) \sim \mathcal{N}(0, 0.5)$ represents the Gaussian noise.

[1] μ and τ regulate the smooth degrees of the output modes and IFs respectively and $\mu = 0.5e{-}8$ and $\tau^1 = 1e{-}8$ are recommended in this paper.

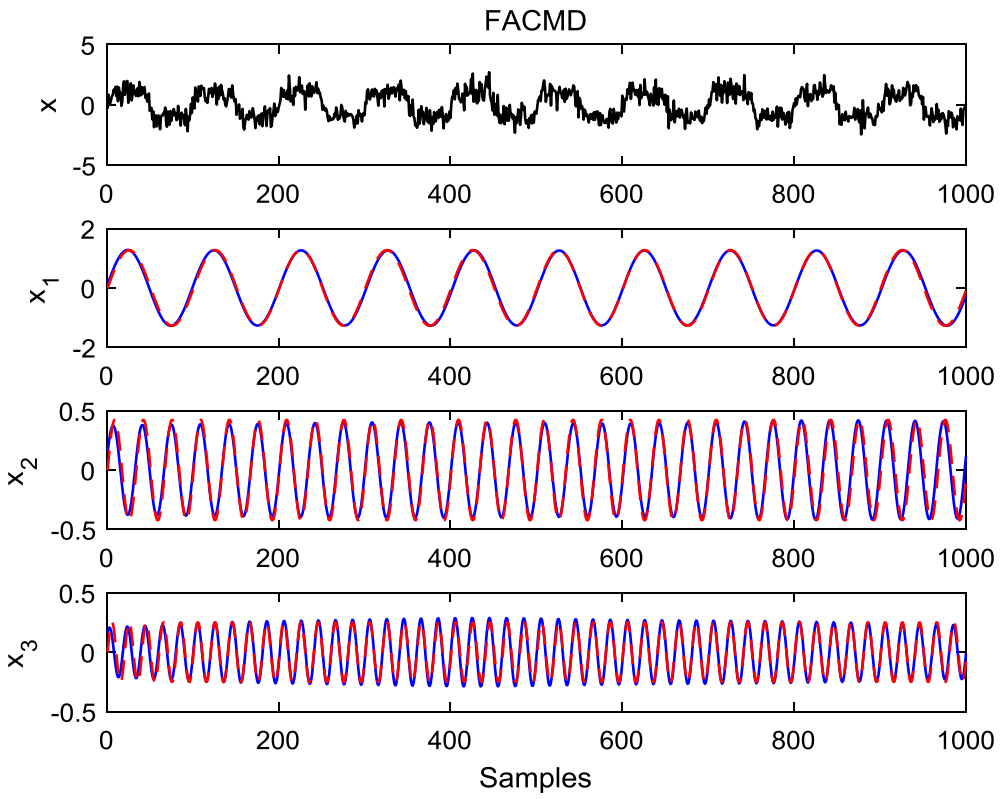

Fig. 2. FACMD decomposition results of the square wave signal. Red dashed lines and blue solid lines represent the real sub-signals contained in $x(t)$ and the modes obtained by decomposition, respectively . (For interpretation of the references to color in this figure legend, the reader is referred to the web version of this article.)

Table 1
Running time and errors of different methods for square wave and time-varying signals.

Signal	Index	FACMD	ACMD	VMD	ITD	LMD	EMD
(Case 1)	Time	**0.9559**	1.6538	0.6557	0.1466	0.0897	0.1082
Square wave	Error	**110.7623**	716.1157	487.5369	921.2327	639.2833	693.8335
(Case 2)	Time	**0.4563**	0.5186	0.6846	0.0111	0.0209	0.0190
Time-varying	Error	**113.8782**	146.3545	884.3469	1725.3421	1835.5768	1364.9656

The decomposition of FACMD and the vanilla ACMD are respectively shown in Figs. 2 and 3. Since the cores of both the proposed FACMD and the vanilla ACMD are derived from VNCMD, their decomposition performances of the first three modes (x_1, x_2, x_3) are similar and satisfactory. However, the vanilla ACMD produces three redundant modes while FACMD nearly perfectly highlights the composition of the original signal. In addition, the running time of the proposed FACMD and the vanilla ACMD is 0.9559 s and 1.6538 s, respectively. Thus, the proposed FACMD indeed speeds up computation as well as reduces redundancy while the same decomposition quality is maintained. Some other typical mainstream decomposition algorithms, including VMD (Dragomiretskiy & Zosso, 2013), ITD (Frei & Osorio, 2006), LMD (Smith, 2005) and EMD (Huang et al., 1998), are also applied; the corresponding performance plots are shown in Figs. 4, 5, 6, and 7, respectively. It can be clearly observed that FACMD is still superior to all the above four classic methods.

Case 2: A time-varying signal in Eq. (14) borrowed from Chen, Yang, Peng, Dong et al. (2019) is tested here.

$$\begin{aligned} x(t) &= x_1(t) + x_2(t) + x_3(t) + \eta(t) \\ x_1(t) &= \mathrm{e}^{-0.03t}\cos\left[2\pi\left(1.3 + 25t + 4t^2 - 0.8t^3 + 0.07t^4\right)\right] \\ x_2(t) &= \mathrm{e}^{-0.06t}\cos\left[2\pi\left(2.6 + 40t + 8t^2 - 1.6t^3 + 0.14t^4\right)\right] \\ x_3(t) &= \mathrm{e}^{-0.09t}\cos\left[2\pi\left(3.9 + 60t + 12t^2 - 2.4t^3 + 0.24t^4\right)\right] \end{aligned} \tag{14}$$

where $\eta(t) \sim \mathcal{N}(0, 0.5)$ represents the white noise.

Table 2
Normalized correlation coefficient of different modes for the square wave.

Mode	λ_{ACMD}	λ_{FACMD}	Harmonic order
1	1	1	1
2	0.3178	0.3178	3
3	0.2064	0.2064	5
4	0.1450	–	7
5	0.1217	–	9
6	0.1139	–	11
7	0.1070	–	13

The decomposition plots of all the algorithms are shown in Figs. 8, 9, 10, 11, 12, and 13, respectively. Even if IAs and IFs are time-varying of these three modes, all the methods except for FACMD and ACMD perform rather poorly. In view of the time-varying property, VMD assumes each mode to be mostly compact around a center pulsation, which limits its ability to track time-varying signals. On the contrary, the cores of FACMD, which are AM-FM modes, make FACMD suitable to express such signals.

In order to quantify the performances of these methods, their corresponding running time and errors are summarized in Table 1. The smaller these two indices are, the better performance the corresponding method has. The error is calculated as $\sum_i^K \sum_j^N \left|x_{i,j} - u_{i,j}\right|$, where $K = 3$ and N denotes the length of modes; $x_{i,j}$ and $u_{i,j}$ stands for the modes obtained by decomposition and real modes in the signal, respectively.

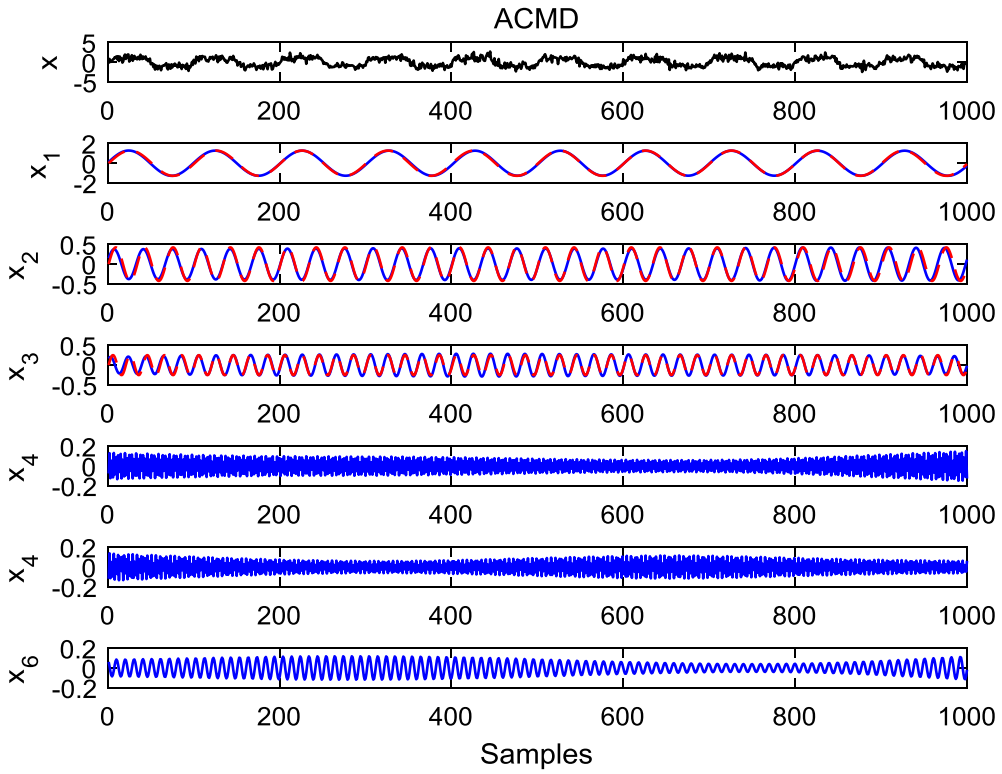

Fig. 3. ACMD decomposition results of the square wave signal. Red dashed lines and blue solid lines represent the real sub-signals contained in $x(t)$ and the modes obtained by decomposition, respectively . (For interpretation of the references to color in this figure legend, the reader is referred to the web version of this article.)

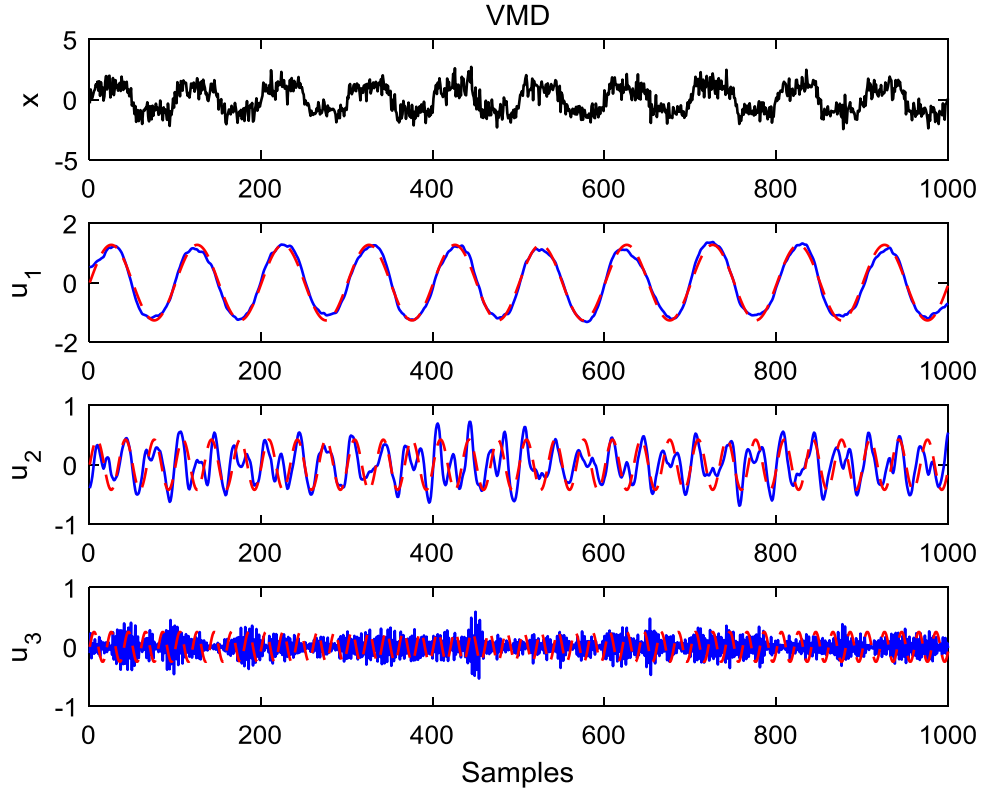

Fig. 4. VMD decomposition results of the square wave signal. Red dashed lines and blue solid lines represent the real sub-signals contained in $x(t)$ and the modes obtained by decomposition, respectively . (For interpretation of the references to color in this figure legend, the reader is referred to the web version of this article.)

In summary, the merits of FACMD contain at least two aspects: (i) The proposed FACMD can adaptively determine the mode number while the other approaches do not. (ii) FACMD outperforms in decomposition quality while the others often suffer from mode-mix or failure. It is

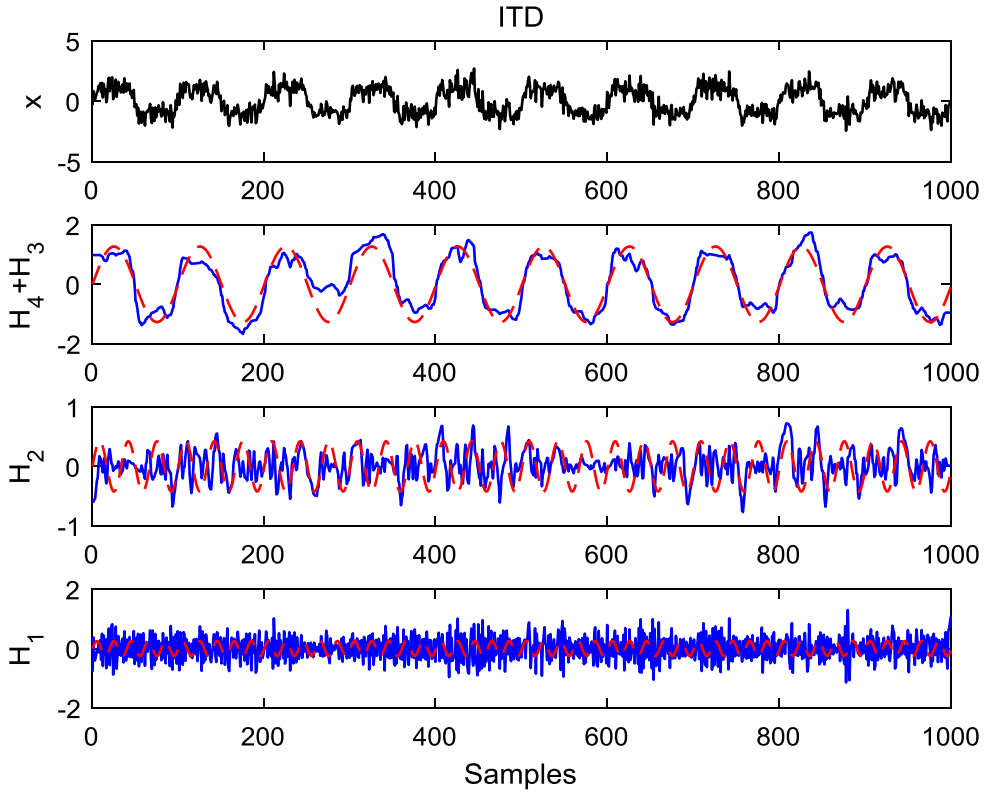

Fig. 5. ITD decomposition results of the square wave signal. Red dashed lines and blue solid lines represent the real sub-signals contained in $x(t)$ and the modes obtained by decomposition, respectively . (For interpretation of the references to color in this figure legend, the reader is referred to the web version of this article.)

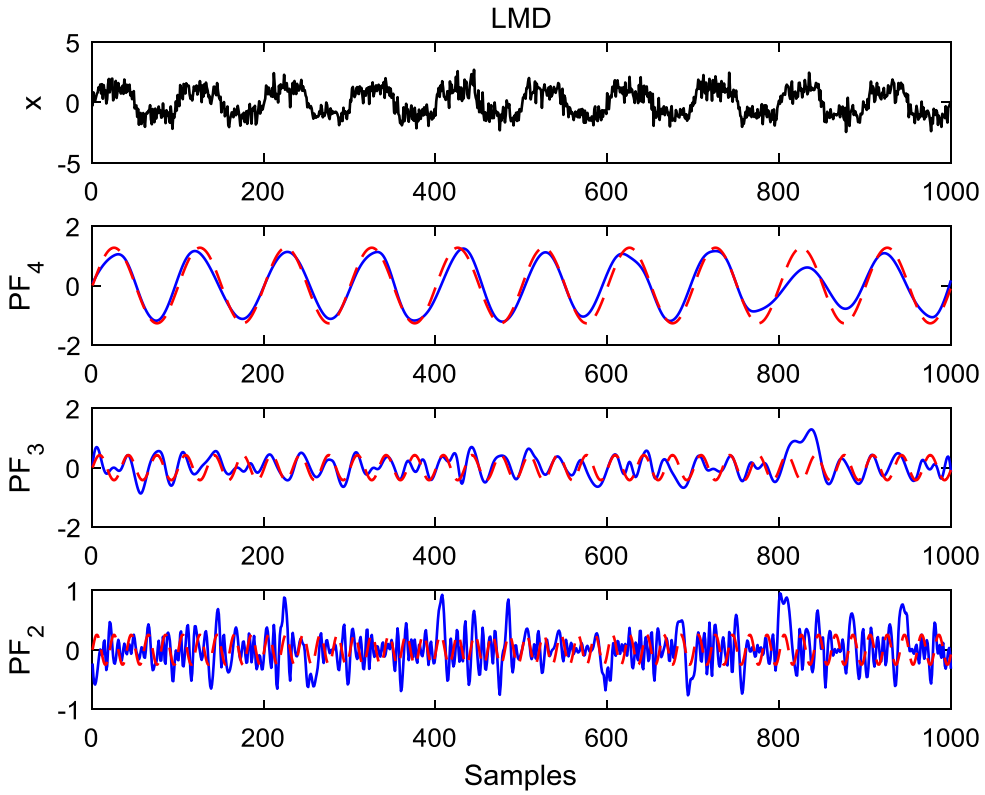

Fig. 6. LMD decomposition results of the square wave signal. Red dashed lines and blue solid lines represent the real sub-signals contained in $x(t)$ and the modes obtained by decomposition, respectively . (For interpretation of the references to color in this figure legend, the reader is referred to the web version of this article.)

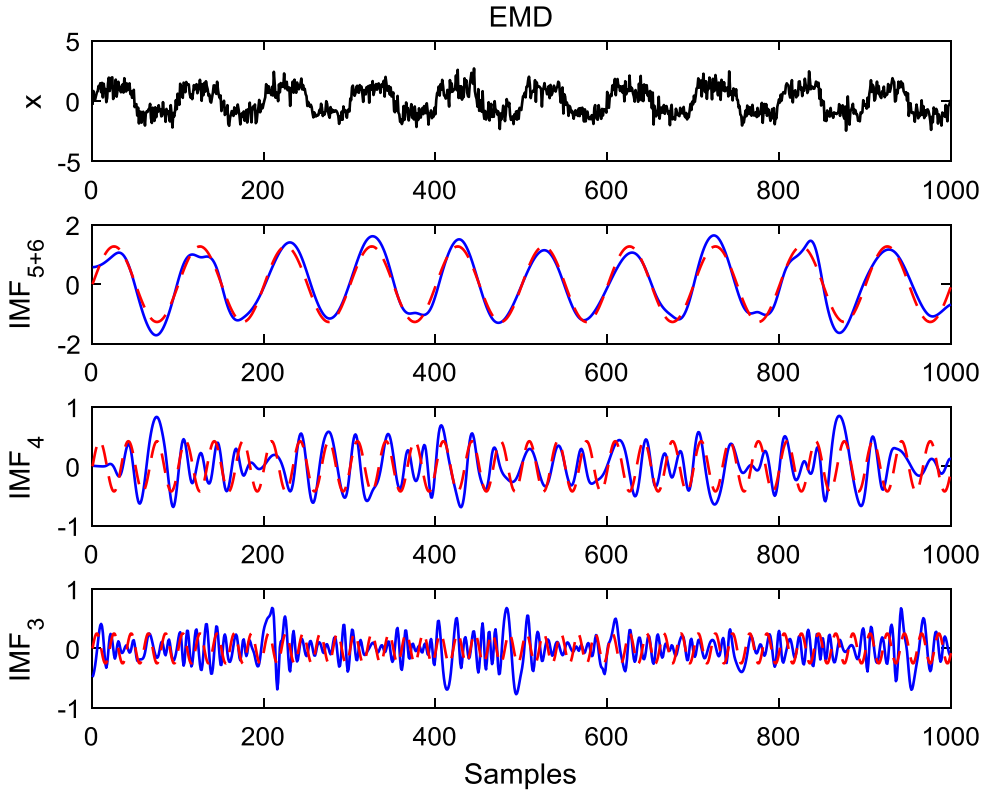

Fig. 7. EMD decomposition results of the square wave signal. Red dashed lines and blue solid lines represent the real sub-signals contained in $x(t)$ and the modes obtained by decomposition, respectively . (For interpretation of the references to color in this figure legend, the reader is referred to the web version of this article.)

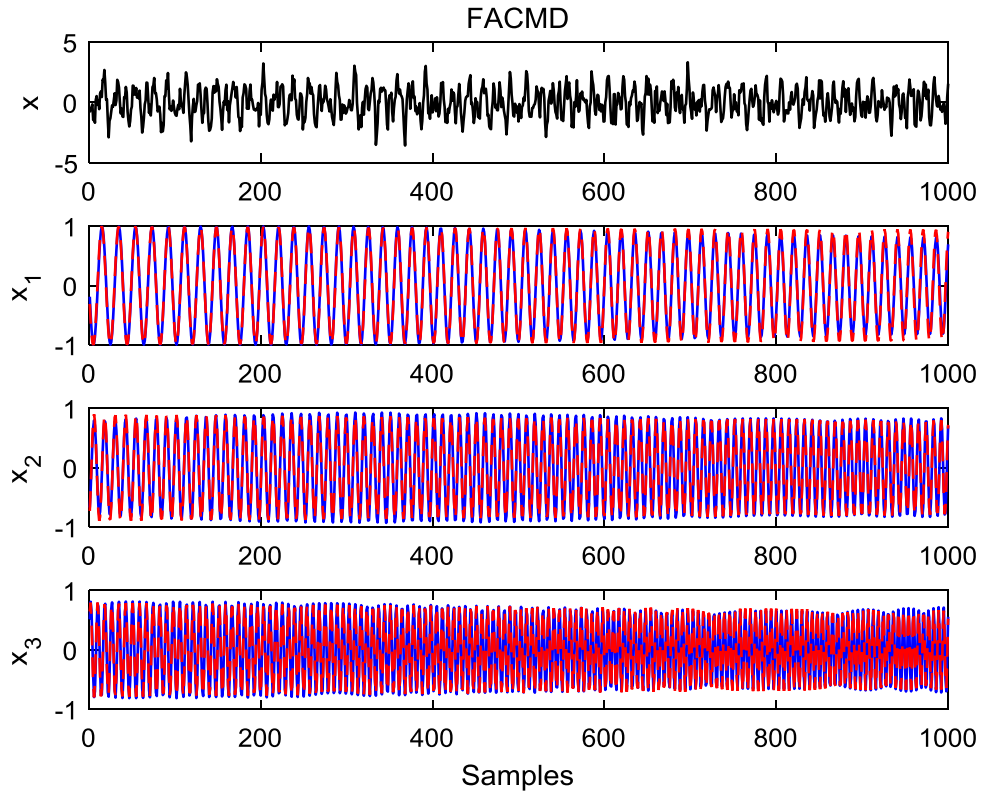

Fig. 8. FACMD decomposition results of the time-varying signal. Red dashed lines and blue solid lines represent the real sub-signals contained in $x(t)$ and the modes obtained by decomposition, respectively . (For interpretation of the references to color in this figure legend, the reader is referred to the web version of this article.)

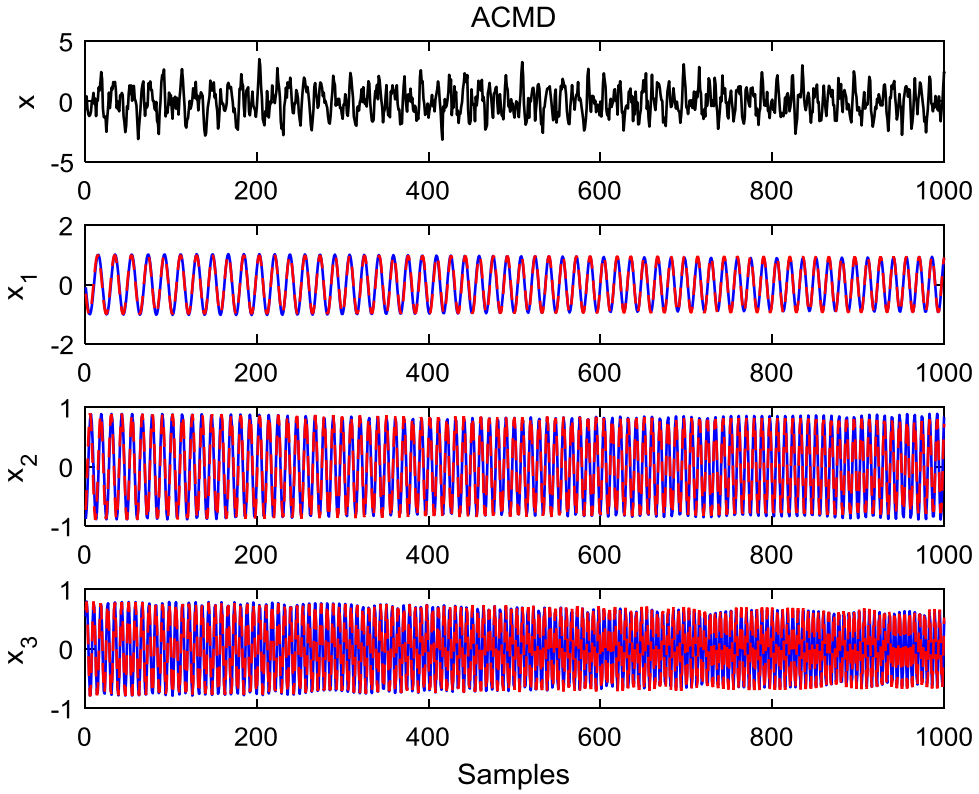

Fig. 9. ACMD decomposition results of the time-varying signal. Red dashed lines and blue solid lines represent the real sub-signals contained in $x(t)$ and the modes obtained by decomposition, respectively . (For interpretation of the references to color in this figure legend, the reader is referred to the web version of this article.)

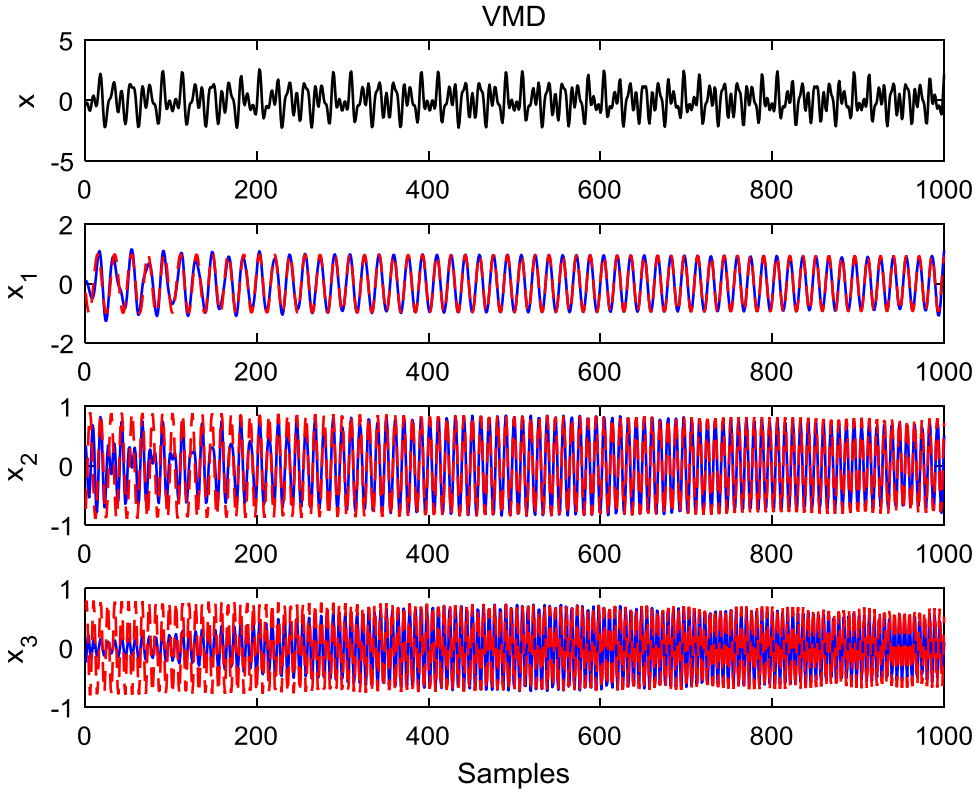

Fig. 10. VMD decomposition results of the time-varying signal. Red dashed lines and blue solid lines represent the real sub-signals contained in $x(t)$ and the modes obtained by decomposition, respectively . (For interpretation of the references to color in this figure legend, the reader is referred to the web version of this article.)

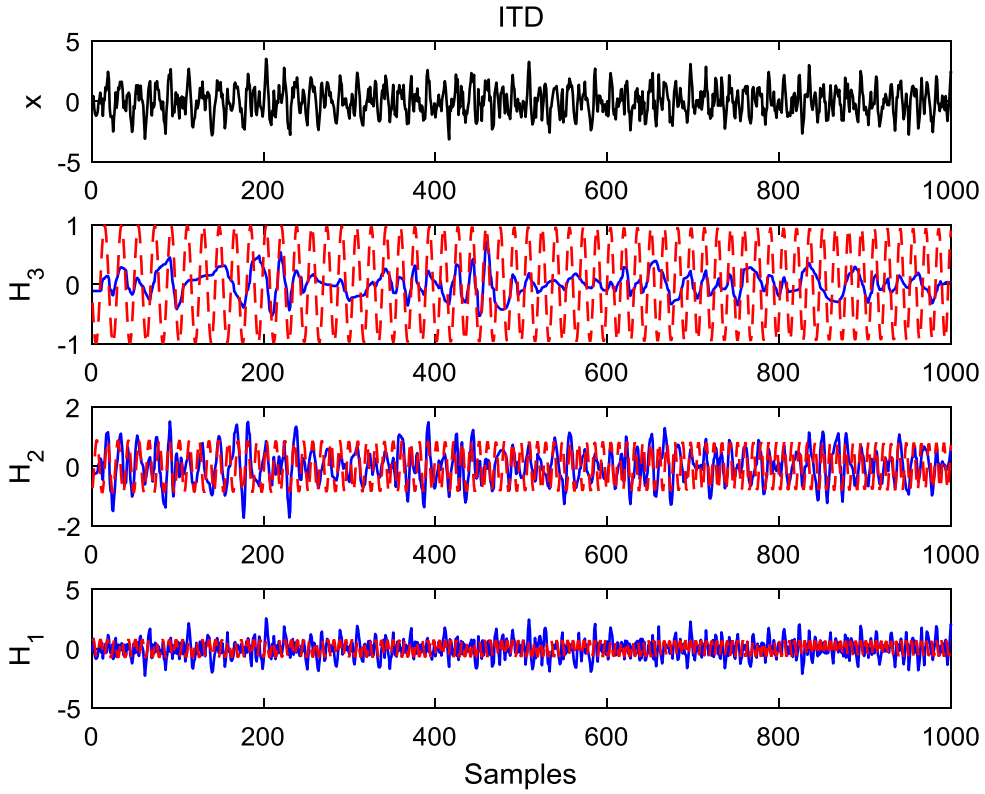

Fig. 11. ITD decomposition results of the time-varying signal. Red dashed lines and blue solid lines represent the real sub-signals contained in $x(t)$ and the modes obtained by decomposition, respectively . (For interpretation of the references to color in this figure legend, the reader is referred to the web version of this article.)

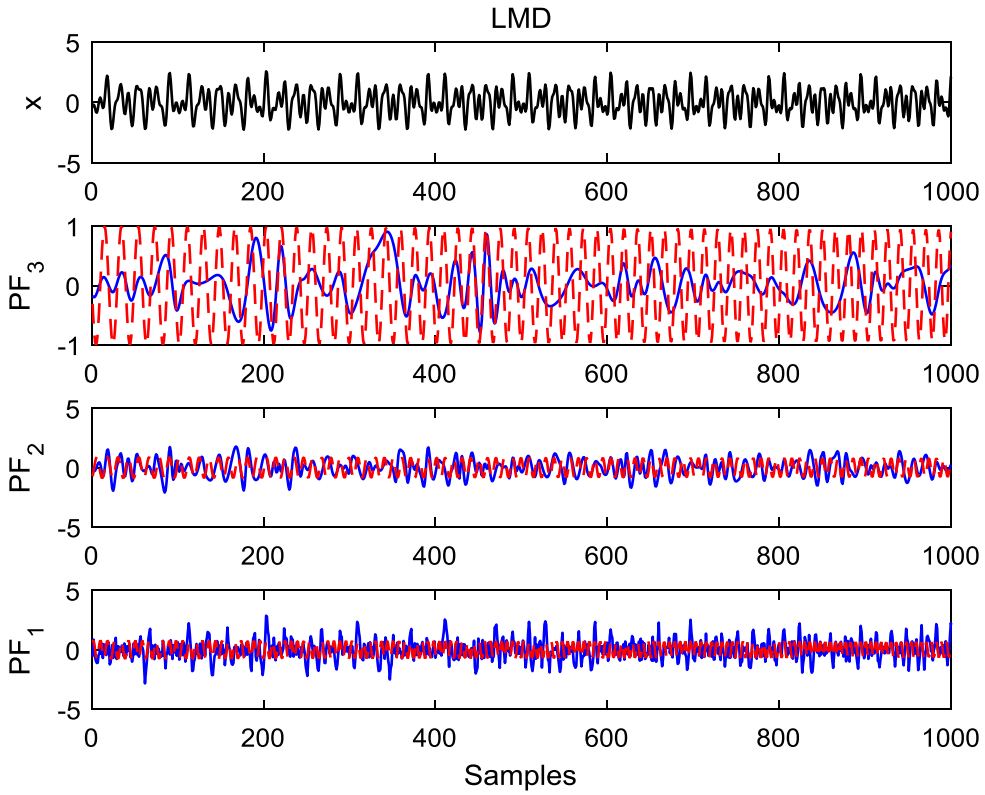

Fig. 12. LMD decomposition results of the time-varying signal. Red dashed lines and blue solid lines represent the real sub-signals contained in $x(t)$ and the modes obtained by decomposition, respectively . (For interpretation of the references to color in this figure legend, the reader is referred to the web version of this article.)

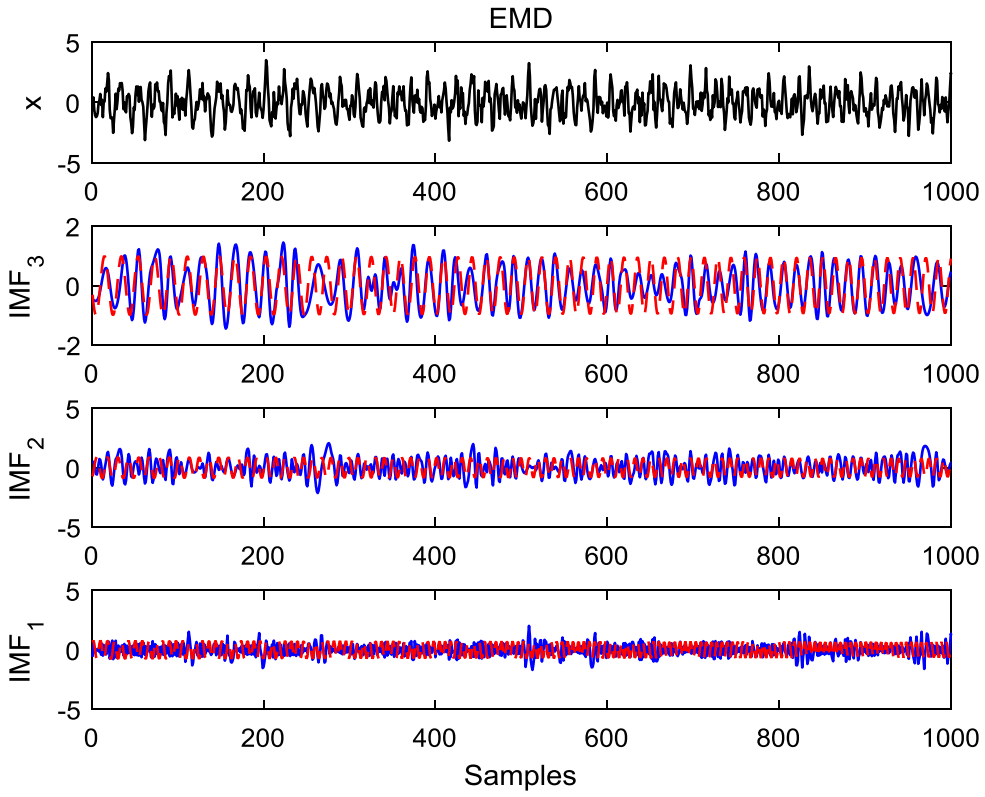

Fig. 13. EMD decomposition results of the time-varying signal. Red dashed lines and blue solid lines represent the real sub-signals contained in $x(t)$ and the modes obtained by decomposition, respectively . (For interpretation of the references to color in this figure legend, the reader is referred to the web version of this article.)

noticeable that when the white noise $\eta(t)$ in Eqs. (13) and (14) becomes colored noise $c\eta(t)$, FACMD can still maintain the best decomposition performance. The colored noise $c\eta(t)$ is generated by passing white noise through the filter $1/\left(1-0.7z^{-1}\right)$ (Li, Wang, Huang, & Lu, 2010; Srinivasan & Rengaswamy, 2012). In addition, unlike the empirical ITD, LMD, and EMD without strong theoretical basis, FACMD is built upon a mature theory and is solved using an optimization scheme. More comparisons on the running time of FACMD and ACMD are provided in Section 5.

3. Oscillation detection

As the proposed FACMD can well decompose the process variable into several significant modes, the next step is to find out which modes have oscillations. To select significant modes and remove the normal operation signals, here the testing significance of oscillation in both time and frequency domains by the consistency function (Wardana, 2015) and the sparseness index (Srinivasan & Rengaswamy, 2012), respectively, are used.

3.1. Oscillation index

The consistency function (Wardana, 2015) is a simple statistics which can quantify the probability of oscillation occurrence for the significant modes. The normalized auto-covariance correlation coefficient, ACF, is first calculated based on the measurement, given by

$$ACF_{x_m} = \frac{1}{N\sigma^2}\sum_{n=1}^{n-v} x_m(n)\,x_m(n+v) \tag{15}$$

where σ^2 is the measurement variance; v and N are the time lag and the length, respectively. The interval of two neighbor zero crossings $(z_m^i, i=1,2,\ldots,N_m)$ represents a half-periods of the oscillation $(T_m^i, i=1,2,\ldots,N_m)$, i.e. $T_m^i = 2z_m^i$, where N_m is the total number of intervals. The consistency function of Eq. (15) can be provided by

$$c_m = \frac{u_{T_m} - \sigma_{T_m}}{u_{T_m}} \tag{16}$$

where u_{T_m} and σ_{T_m} are the mean and the standard deviation of T_m^i, respectively. Eq. (16) clearly indicates that the corresponding variance will be large, resulting in $u_{T_m} - \sigma_{T_m}$ is less than u_{T_m} if the intervals $(z_m^i, i=1,2,\ldots,N_m)$ are not uniform. Conversely, the variance (σ_{T_m}) is small and it would approach 0; c_m is approximately equal to 1. Thus, the more regular the oscillation period is, the closer to 1 the index (c_m) is. In this paper, only modes with $c_m > \mu_c$ are retained for further analysis, where $\mu_c = 0.95$ is recommended (Wardana, 2015).

The ideal oscillatory signal should have one peak only at the specific frequency (X_m) while it has zero magnitude at all the other frequencies. To confirm the presence of oscillations in the frequency domain, the vector containing the magnitude of the oscillatory signal at various frequencies obtained from Fourier transform should be sparse. Its magnitude of the energy ratio can be measured by the sparseness index (SI) (Srinivasan & Rengaswamy, 2012), given in Eq. (17).

$$SI_m = \frac{\sqrt{N} - \left(\sum_{i=1}^{N}|X_m^i| \Big/ \sqrt{\sum_{i=1}^{N}|X_m^i|^2}\right)}{\sqrt{N}-1} \tag{17}$$

where X_m^i is the frequency response of x_m and N is the length of the vector. Eq. (17) indicates that $SI_m = 1$ if there is only one peak in the spectrum X_m and zero magnitudes are zeros at all the other frequencies. In the other extreme condition, $SI_m = 0$ when the amplitude at each frequency is equal and non-zero (such as white noise). Thus this index (SI_m) is used to represent the sparsity of spectrum. The sparser the spectrum is, the more obvious the peak value is. A clear peak in the spectrum corresponds to the confirmed oscillations in the time domain. In this paper, if a PV contains the modes with $SI_m > \mu_{SI}$, then the oscillations are detected and the corresponding loop is thought to be oscillatory. According to Aftab et al. (2017), $\mu_{SI} = 0.58$ is adopted.

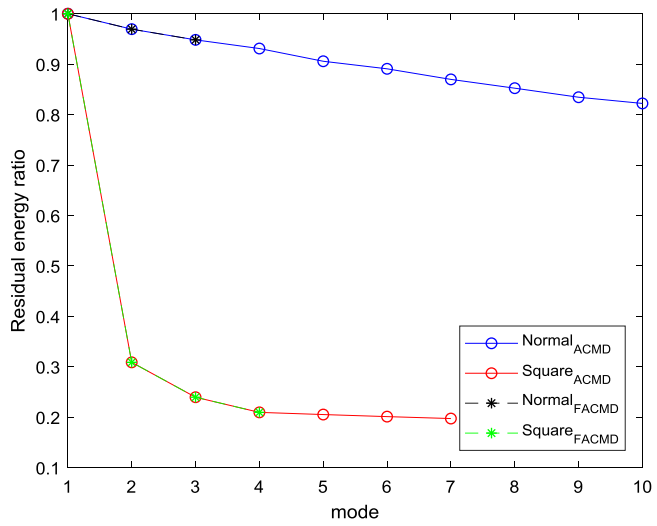

Fig. 14. Residual energy ratio of the normal and square (oscillating) cases . (For interpretation of the references to color in this figure legend, the reader is referred to the web version of this article.)

3.2. Discussion on thresholds

A total of four thresholds is used in the previous sections, including the energy ratio threshold μ_n, the normalized correlation coefficient threshold μ_λ, the consistency function threshold μ_c, and the sparseness index threshold μ_{SI}. The first two thresholds (μ_n and μ_λ) measure the relationship between the modes and the original signal. They can be changed with different decomposition algorithms while the other two (μ_c and μ_{SI}) only quantify the oscillation degree of a single time series itself regardless of the way the series generates. Their default settings are briefly discussed below.

3.2.1. Energy ratio threshold (μ_n)

The energy ratio index (Eq. (12)) is adopted to remove the normal mode whose process values should be a constant theoretically from the measured signals. However, because of the presence of noise in the actual industrial plant, the normal process values are usually contaminated by noise, which makes the energy ratio index unreliable to distinguish the normal from the oscillating conditions with naked eyes. Since ACMD is an extended version of VMD, both of them have an equivalent filter bank structure (Wang & Markert, 2016). If the process signals have white noise (normal), the corresponding energy of these modes will have almost equal energy. Thus the residual energy ratio will approximate linear decay in the iteration procedure as shown in Fig. 14. On the contrary, the difference in the energy values between the modes is very large when oscillations occur, which leads to the rapid decay of the residual energy ratio. It could be observed that $\mu_n = 0.9$ can well separate the normal from the oscillating conditions with large margins. In addition, the vanilla ACMD decomposes the normal case into too many redundant components while the proposed FACMD can successfully avoid this drawback by terminating the outer loop prematurely. This is also one of the acceleration principles of the proposed FACMD.

3.2.2. Correlation threshold (μ_λ)

The normalized correlation coefficient (Eq. (11)) is used to discard the spurious modes generated by decomposition. Its threshold is a trade-off between the number of discarded modes and avoiding loss of effective information. This threshold can be determined in a way similar to Aftab et al. (2017). The tested signal is a square wave like Eq. (13), but the order of harmonics is up to 13. The corresponding normalized correlation coefficients of different modes are listed in Table 2. It can be inferred that the threshold $\mu_\lambda = 0.15$ will enable the proposed FACMD to characterize the fifth harmonic, which is sufficient for oscillation detection and diagnosis (Aftab et al., 2017). In addition, this threshold can avert over-decomposition by terminating the outer loop prematurely, too. It is worth noting that more testings in Section 5 will validate their effectiveness fully although the thresholds μ_n and μ_λ are discussed only in one typical example here.

3.2.3. Consistency function (μ_c) and sparseness index threshold (μ_{SI})

As stated above, both the consistency function (Eq. (16)) and the sparseness index (Eq. (17)) are not dependent on both the original signal and the decomposition algorithm. The existing conclusions (Aftab et al., 2017; Wardana, 2015), i.e. $\mu_c = 0.95$ and $\mu_{SI} = 0.58$, are adopted directly in this paper.

Therefore, the procedure of the proposed oscillation detector can be described as: Firstly, the process variable is decomposed into several modes by the FACMD, and the normal signals are also removed. Then the presence of oscillation can be identified and confirmed both in time and frequency domains by the consistency function (Eq. (16)) and the sparseness index (Eq. (17)), respectively. If the mth mode satisfies the condition $c_m > \mu_c$ or $SI_m > \mu_{SI}$, the oscillation is detected in the corresponding loop. Otherwise, this loop is in the normal operation. The illustrative examples are further discussed in Section 5.

4. Oscillation diagnosis

The previous section discussed the oscillation detection using the proposed FACMD, which identifies the decomposed modes with oscillation behaviors. Although the method assists in diagnosing the fault cause, it may take a substantial amount of time and process expertise before the fault is properly diagnosed. To effectively identify the fault causes in the control loops, the nonlinearity-induced oscillations are firstly detected by checking the frequency relationships among different modes in this section. After the modes related to nonlinear oscillations are removed, the retained oscillatory modes are further classified into two types of linear oscillations, i.e. external harmonic disturbances or oscillations induced by poor controller tuning, by a hypothesis test.

4.1. Diagnosis of nonlinear oscillations

Oscillations caused by nonlinearity, such as control valve stiction, have the distinct property of being nonlinear, which makes them distinguishable from the other types of oscillations (Choudhury, Shah, & Thornhill, 2008). Proceeding from the fact that nonlinearity-induced oscillations contain higher order harmonics (Aftab et al., 2017), the nonlinearity can be identified by checking the frequency relationships among different modes. According to Aftab et al. (2017), it should be noted that the mode containing the fundamental frequency of oscillations has a higher correlation with the decomposed process variable than its harmonics, i.e.

$$\lambda_f > \lambda_{h_i},\ i \in \mathrm{Z}^+ \tag{18}$$

where λ_f and λ_{h_i} represent the normalized correlation coefficient of fundamental and the ith order harmonic mode, respectively. The correlation coefficient can be calculated by the input IF_i, which is the instantaneous frequency of oscillatory modes obtained from Algorithm 2. By a logical extension of this point, the correlational relationship of different order harmonics induced by the same nonlinearity source must satisfy the following condition,

$$\lambda_{h_{i+1}} < \lambda_{h_i},\ i \in \mathrm{Z}^+ \tag{19}$$

where λ_{h_i} and $\lambda_{h_{i+1}}$ stand for the normalized correlation coefficient of the ith and the $(i+1)$th order harmonics, respectively. Thus, if two modes meet Step 5 in Algorithm 3 instead of the condition in Eq. (19), they may be caused by different nonlinear sources. The above two

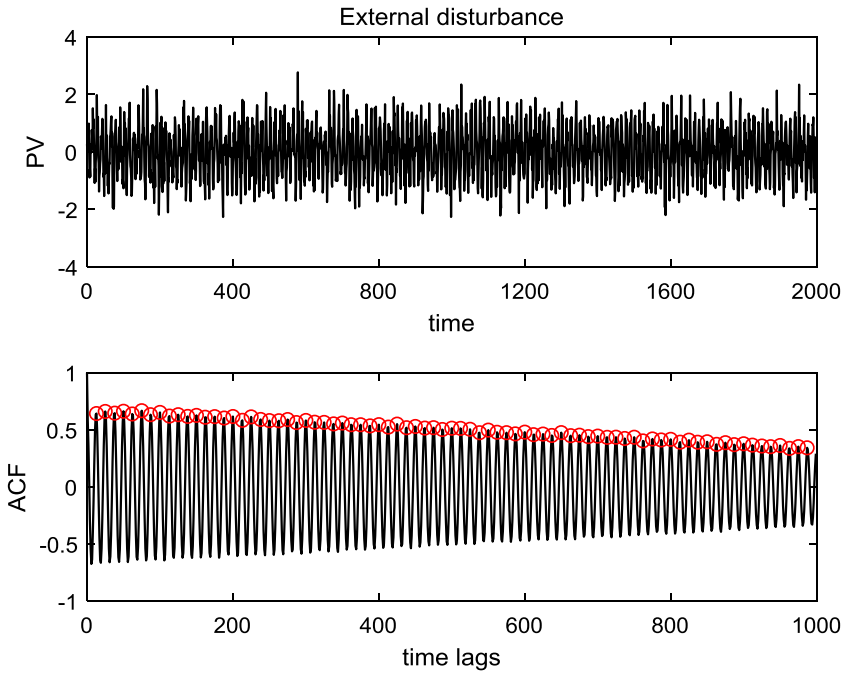

Fig. 15. External harmonic disturbance and its ACF.

conditions (Eqs. (18)–(19)) are able to distinguish nonlinearity-induced oscillations arising from multiple sources.

Algorithm 3 depicts the corresponding diagnosis procedure in detail. Although the proposed Algorithm 3 and the method in Aftab et al. (2017) are all based on the decomposition modes, it is worthy of pointing out that two things are different in substance. Firstly, Algorithm 3 is based on the instantaneous frequency of the whole time to examine the frequency relationship among different modes. While the MEMD-based technique just estimates the frequency by calculating 11 successive zero-crossings. This means the diagnosis results of the proposed Algorithm 3 are much more accurate and reliable. Secondly, MEMD lacks the theoretical principle. Its performance and efficiency highly depend on the projection number and the direction. These problems still have not been solved (Lang, Zheng et al., 2018). Instead, FACMD is computationally efficient and theoretically well-founded.

Algorithm 3: Diagnosis of nonlinear oscillations

Input: IF_i and λ_i of the oscillatory modes, $i = 1,2,3,\ldots$

Output: nonlinearity-induced oscillating modes

1: calculate the mean frequency of IF $IF_{mean_i} = mean(IF_i)$, and the corresponding upper and lower limits of confidence intervals $IF_{max_i} = 1/(IF_{mean_i} - std(IF_i))$, $IF_{min_i} = 1/(IF_{mean_i} + std(IF_i))$

2: regard the mean frequency of the most correlated modes as fundamental frequency, denoted as $IF_{mean_{max}}$

3: **for** $i \in Z^+$ and $i \neq \lambda_{max}$ **do**

4: **if** $IF_{min_i} \leq k \times IF_{mean_{max}} \leq IF_{max_i}$, $k \in Z^+$ and $k > 1$ **then**

5: Mode i and λ_{max} are nonlinearity-induced oscillations

6: **end if**

7: **end for**

8: in case no nonlinearity-induced oscillation are detected for the most correlated mode, set $IF_{mean_{max}}$ equal to the mean frequency of the next most correlated modes, then repeat the above ``for'' loop (step $4 \sim 8$), and so on;

4.2. Diagnosis of linear oscillations

If the oscillatory modes obtained by FACMD are not induced by nonlinearities, they would be considered as linear oscillations. Because of the effect of noise, the time series plot of an external harmonic disturbance is similar to that of an oscillation introduced by poor controller tuning (Figs. 15 and 16). This makes these two different types of oscillations indistinguishable in the time domain. However, in Fig. 15, ACF of the external harmonic disturbance is constantly oscillating while that of the other signal fades away after a few lags. In Fig. 16, the poor controller tuning induced oscillation has a varying amplitude in its corresponding ACF (Naghoosi & Huang, 2014b). Naghoosi and Huang (2014b) showed that an oscillation caused by poor controller tuning has different autocorrelation functions (ACFs) (Eq. (15)) (15) from an external harmonic disturbance with the same frequency. Based on these two different characteristics of ACF, an automatic and reliable hypothesis test is developed to diagnose which type of linear oscillation occurs.

The ACF of an external harmonic disturbance $\cos(2\pi\omega t)$ with noise can be predicted as

$$p_r \frac{N-\upsilon}{N-\upsilon_r}\cos(2\pi\omega\upsilon) \tag{20}$$

where p_r is the peak value in ACF and υ_r is its corresponding time lag. The decay caused by the estimation technique results in the difference between the peaks. To compensate the difference, Naghoosi and Huang (2014b) proposed to compare the peak value at the larger lag (p_2) with the adjusted peak value (p_1^a) at the smaller time lag (p_1), in which p_1^a is provided by:

$$p_1^a = p_1 \frac{N-\upsilon_{p_2}}{N-\upsilon_{p_1}}. \tag{21}$$

Thus, $p_2 - p_1^a$ will be no longer affected by the decay induced from estimation. Also, it follows the normal distribution, given by

$$p_2 - p_1^a \sim N\left(0, \frac{1}{N}\left(\frac{\sigma_{noise}^2}{\sigma_{noise}^2+\sigma_{harmonic}^2}\right)^2\left(1+\left(\frac{N-\upsilon_{p_2}}{N-\upsilon_{p_2}}\right)^2\right)\right). \tag{22}$$

If the estimation of the factor $\sigma_{noise}^2/\sigma_{noise}^2 + \sigma_{harmonic}^2$ is not available, an approximate confidence interval equal to $3\sqrt{2}/\sqrt{N}$ can be used to check if the differences between the peak values in ACF are significant. The null hypothesis is that the oscillation is an external harmonic disturbance, not poor controller tuning. If the difference between two peaks in ACF does not exceed the significant level, the oscillation is considered to be an external harmonic disturbance. If the difference exceeds the significant level, the oscillation would not be an external harmonic disturbance. The corresponding distributions of the difference between the peak values in ACF for external harmonic

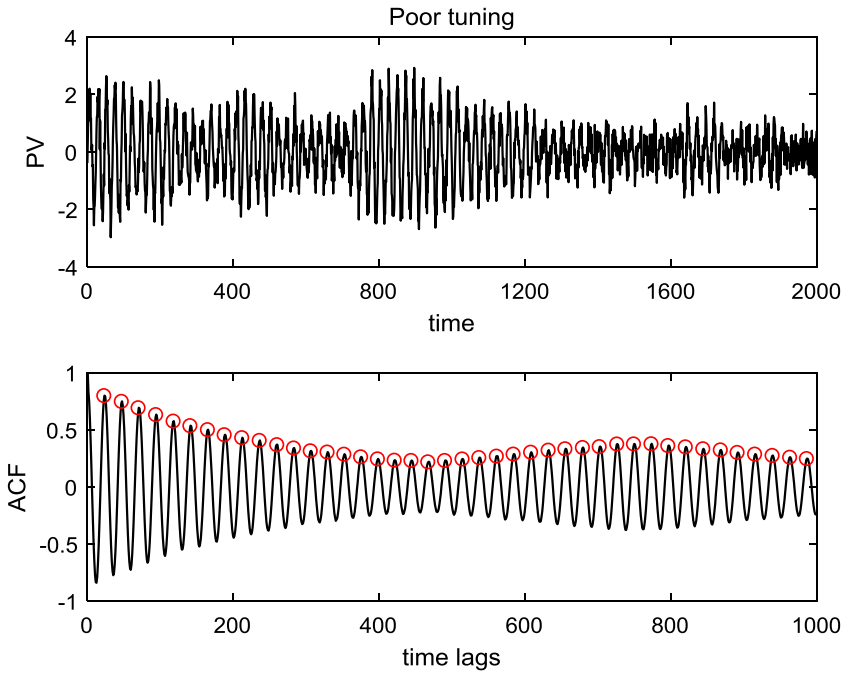

Fig. 16. Poor controller tuning induced oscillation and its ACF.

(a)

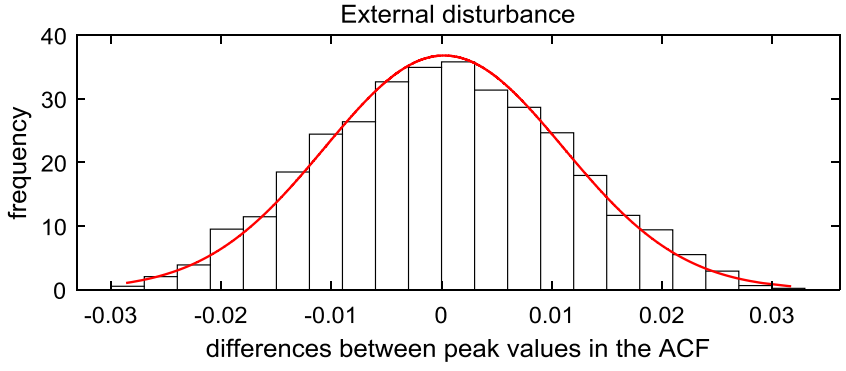

(b)

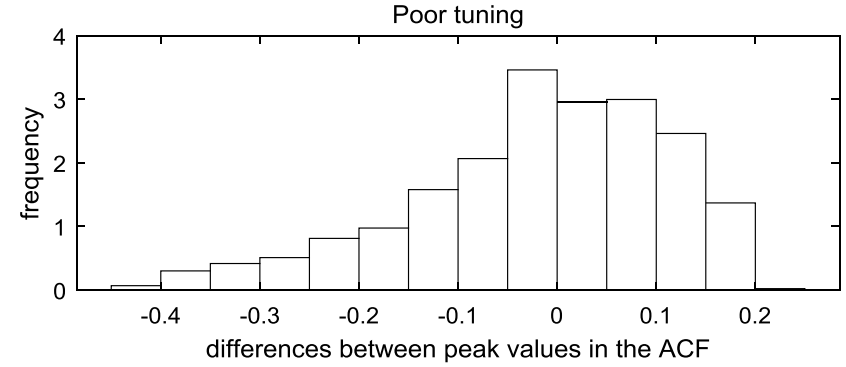

Fig. 17. Distribution of the differences between the peak values in ACF (a) for poor tuning and (b) for external disturbance . (For interpretation of the references to color in this figure legend, the reader is referred to the web version of this article.)

disturbances and poor controller tuning are depicted in Fig. 17(a) and (b), respectively. It is clear that the distribution of the external harmonic disturbance is normal while the others are not.

Based on the above hypothesis test, the retained oscillatory modes, which are not induced by the nonlinearity, can be classified into two

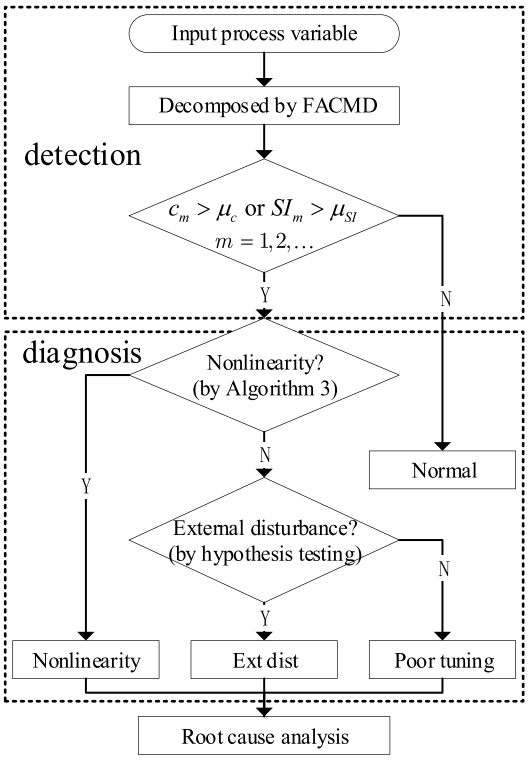

Fig. 18. Flowchart of the proposed FACMD-based detection and diagnosis algorithm.

different types of linear oscillations. The proposed method is an extension to Naghoosi and Huang's method (Naghoosi & Huang, 2014b). It can distinguish a combination of two types of linear oscillations or multiple oscillations while Naghoosi and Huang's work (Naghoosi & Huang, 2014b) is limited to processing single linear oscillation. Recently, Naghoosi and Huang also proposed a wavelet-based methodology to detect and characterize multiple oscillations (Naghoosi & Huang, 2017), but the experimental studies in this paper show that the proposed FACMD scheme outperforms Naghoosi and Huang's method in terms of diagnosis accuracy and the automatic level. Although the similar work based on VMD (Dewa et al., 2018) can diagnose multiple oscillations, it has at least three shortcomings. Initially, only two modes of VMD are utilized, which results in information loss. Secondly, the performance of VMD highly depends on its parameters (mode number and penalty coefficient). Last, the basic mode of VMD is $a(t)\cos(\omega t)$, in which ω represents the center frequency and it is a constant. Thus ω is essentially limited in its ability to accurately express time-varying signals; particularly, the oscillations induced from poor tuning vary with time. On the contrary, the FACMD is represented by $a(t)\cos\left(2\pi\int_0^t f(s)\,ds + \phi\right)$, where f is a time-varying function well suited to depict the complex signals with time-varying characteristics.

To sum up, the components (the controller, the control valve, the process, and the sensor) in the feedback control loops may all suffer from certain abnormalities. The problems may cause degradation of the control performance, such as a large variation of process variables, loop oscillations. The proposed framework for oscillation detection and diagnosis is depicted in Fig. 18. In the oscillation detection, the process variable is decomposed by FACMD into several significant modes and the oscillatory ones are identified by the consistent function (Eq. (16)) and the sparseness index (Eq. (17)). In oscillation diagnosis, the nonlinearity-induced oscillations are detected by Algorithm 3 using higher order harmonics; the retained linear oscillating modes are further distinguished by a hypothesis test of normal distribution. With the above procedure, the underlying sources of the problematic control performance based on the outputs of all the monitors can be systematically and clearly determined.

5. Case studies

5.1. SISO feedback control loop

In order to show the high computational efficiency of FACMD and validate the effectiveness of the proposed detection and diagnosis methodology, a simulated single input and single output (SISO) closed-loop system is borrowed from Aftab, Hovd, Huang, and Sivalingam (2016), Aftab et al. (2017) and displayed in Fig. 19. The nonlinearity is modeled by the two-parameter valve stiction model (Choudhury, Thornhill, & Shah, 2005) with stickband ($S = 7$) and slip jump ($J = 5$) and the plant transfer function is $G(s) = 2.25e^{-3s}/4.54s + 1$. The process is regulated by a PI controller and a white noise with variance 0.1 is added to its outputs. Six different cases are studied successively in total, including (i) a normal condition, (ii) external disturbances, (iii) poor tuning, (iv) combination of external disturbances and poor tuning, (v) nonlinearity/stiction, and (vi) stiction with external disturbances. Their corresponding responses of process variables in all cases are shown in Fig. 20.

(i) Normal operation

In this case, the PI controller parameters are tuned as $K_c = 0.1$ and $I = 0.5$, which makes the loop work in the normal condition. The top of Fig. 20 displays its corresponding time series of the controlled variable. The detection results of the first 3 modes by the proposed FACMD are listed in Table 3. It is concluded that no oscillation is detected in this

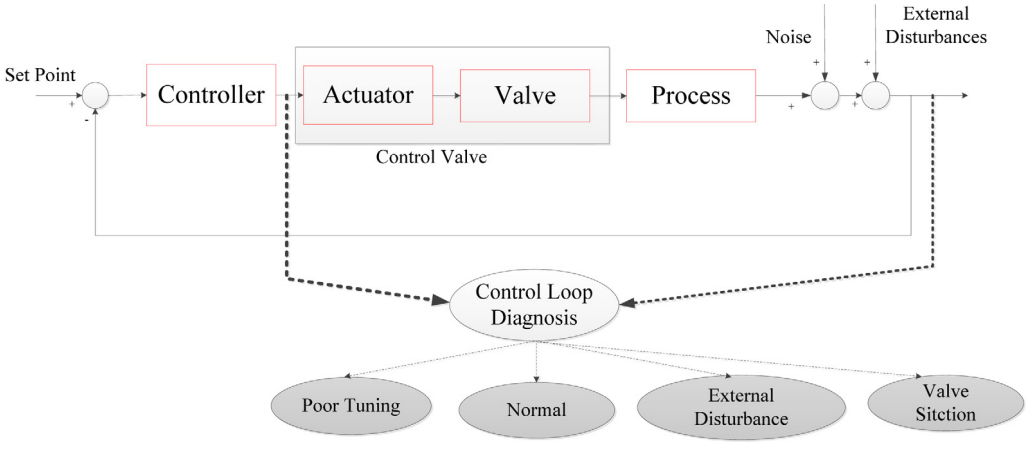

Fig. 19. Simulated SISO control loop.

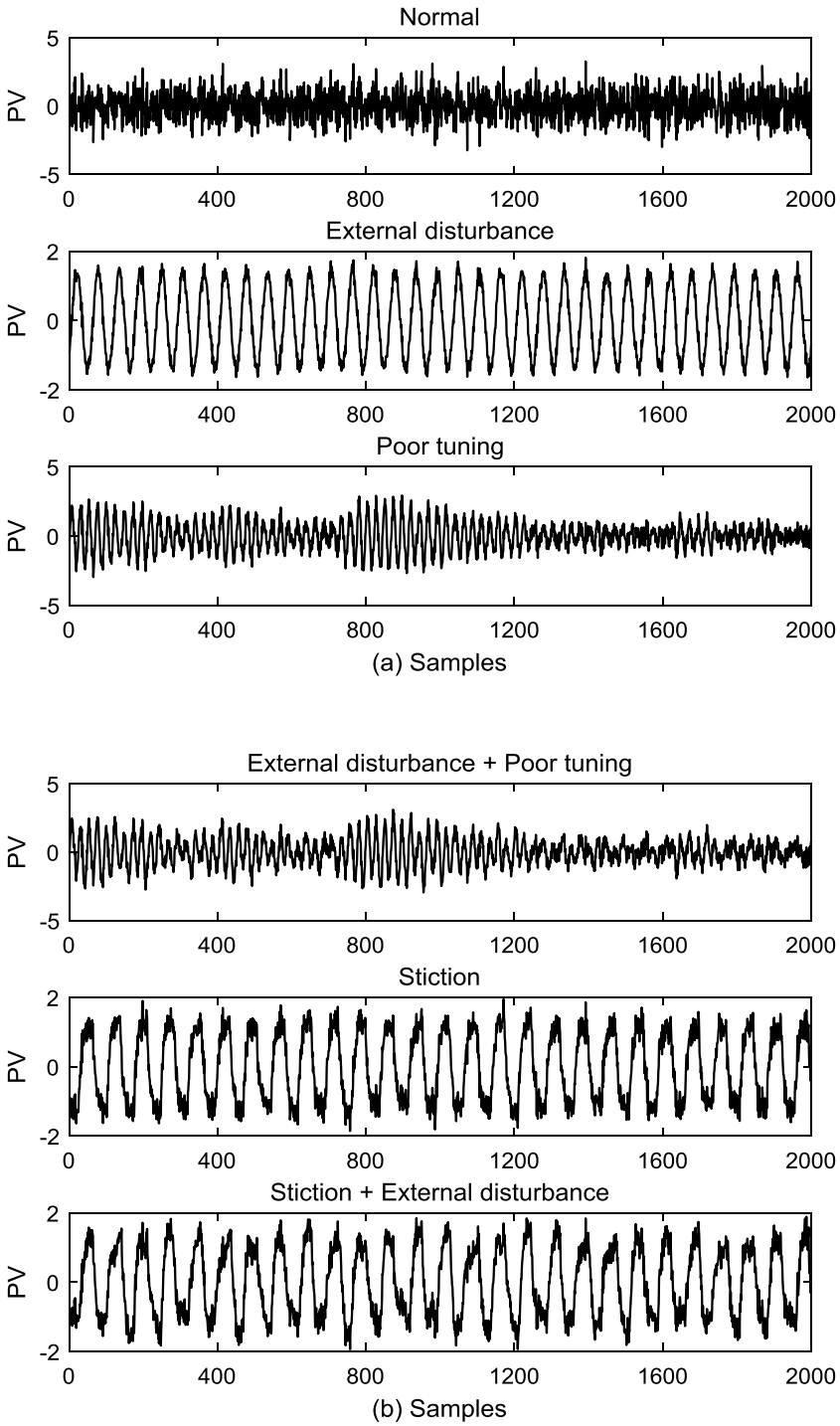

Fig. 20. (a) and (b) show data of six different cases in the simulated SISO system.

loop; thus the proposed method is capable of identifying the normal condition correctly.

(ii) External disturbance

Assume that an external disturbance is a sinusoid signal with 0.0175 Hz. The external harmonic disturbance of the controlled variable causes fluctuations of the control loop. The system response and the decomposition results are shown in Fig. 21, respectively. It is apparent that only one mode is extracted as an oscillating component because of both its consistent function $c_m > \mu_c$ and sparseness index $SI_m > \mu_{SI}$ in Table 3. In the following linear oscillation testing, the hypothesis testing result (as shown in the 2nd case of Table 4) does not reject the null hypothesis, so the presence of presupposed external disturbance (with frequency approximating 0.175 Hz) is confirmed clearly.

(iii) Poor tuning

In this scenario, the controller parameters are tuned as $K_c = 0.1$ and $I = 1.8$ to generate another type of linear oscillation, which can be observed at the top of Fig. 22. In contrast to the normal case, this controller has an excessive integral action. The corresponding decomposition graphs are also depicted in Fig. 22. From the results in Table 3, it can be seen that the consistency functions and sparseness indices of all the three modes excess the prescribed thresholds, which means they

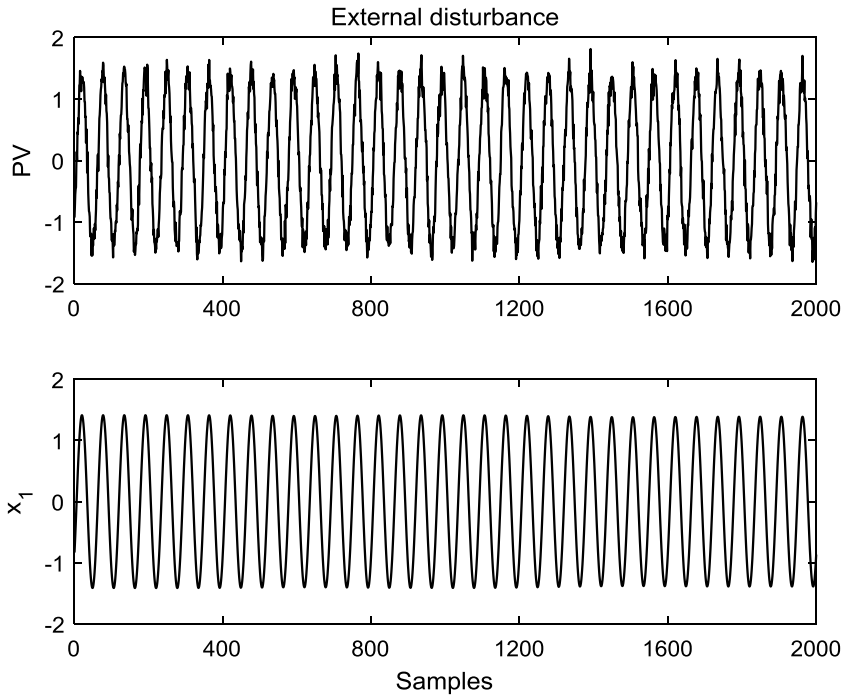

Fig. 21. Decomposition results of external disturbances.

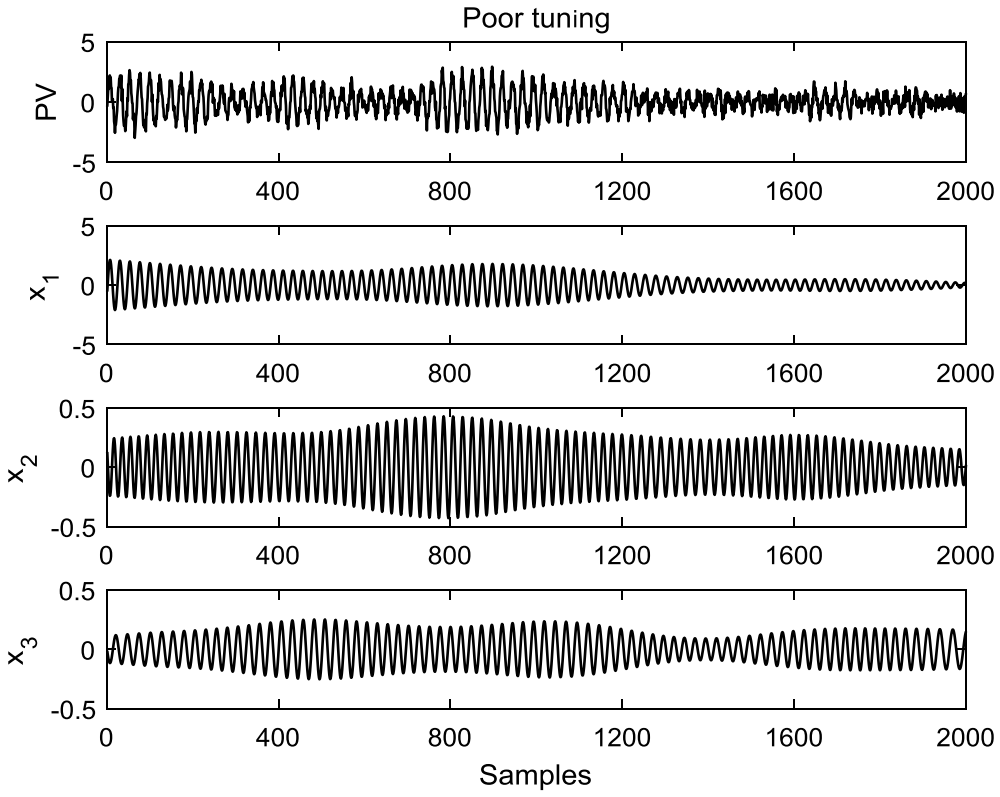

Fig. 22. Decomposition results of poor tuning.

are oscillating components. Since the frequencies of mode 1, 2, and 3 are very close (as shown in Table 4), they can be combined together to carry out hypothesis testing. The conclusion supports the rejection of the null hypothesis, and it can be inferred that the oscillation is introduced by poor controller tuning.

(iv) External disturbance and poor tuning

This example consists of two types of linear oscillations, i.e. the combination of Case (ii) and (iii). Fig. 23 shows the decomposition outputs and the corresponding detection. Since both two oscillation indices of these four modes in Table 3 exceed the prescribed limits, they are diagnosed in accordance with Fig. 23. Firstly, no harmonics are captured, so the presence of nonlinearity is excluded. Like Case (iii), the

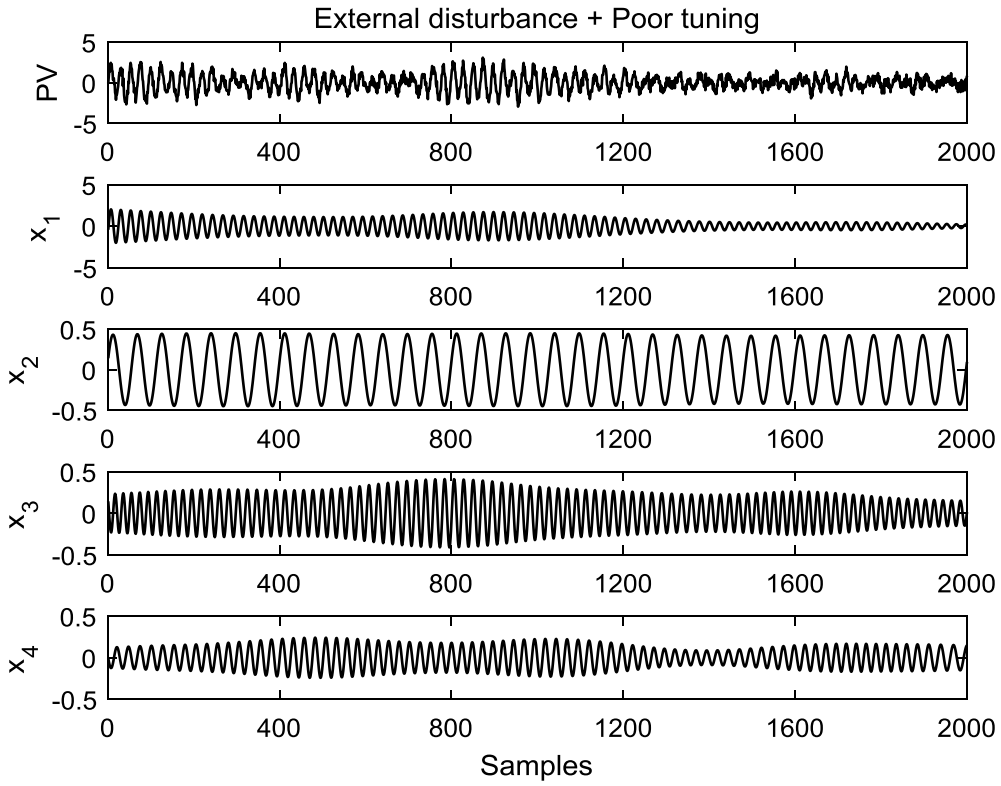

Fig. 23. Decomposition results of the combination of external disturbances and poor tuning.

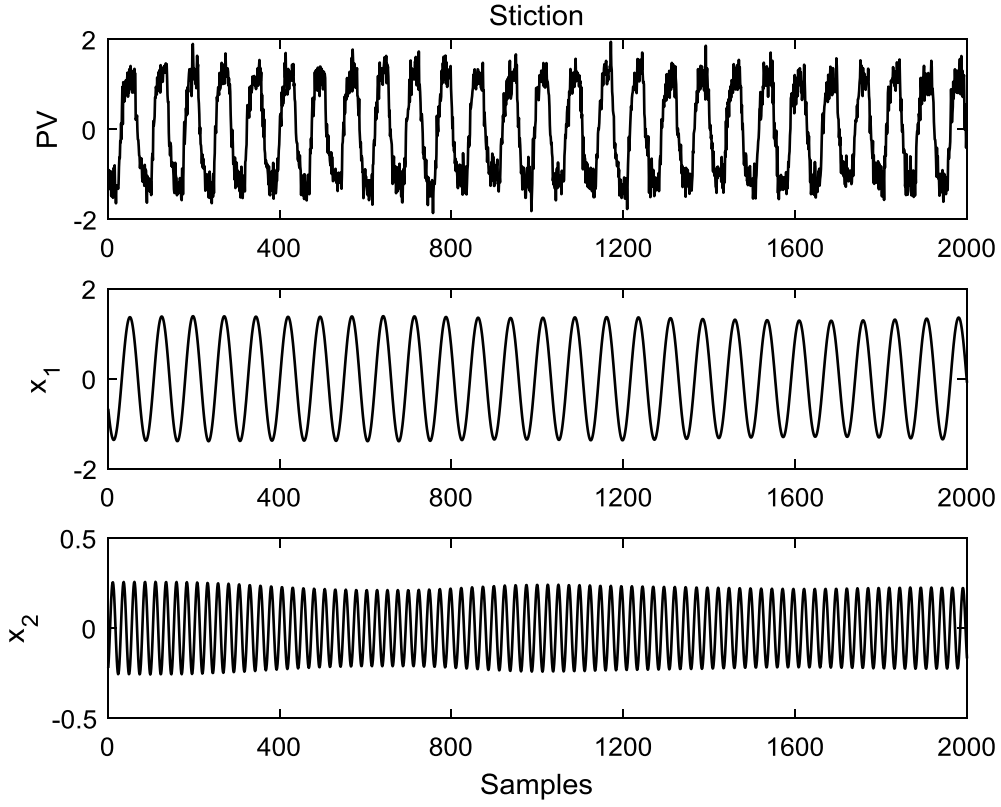

Fig. 24. Decomposition results of valve stiction.

frequencies of mode 1, 3, and 4 are very close; they are added together for linear hypothesis testing. The results in Table 4 show that x_2 accepts the null hypothesis while the others reject the null hypothesis; i.e. x_2 is an external disturbance while the other three modes are oscillations caused by poor controller tuning. Therefore, these conclusions validate the ability of the proposed method to distinguish two types of linear

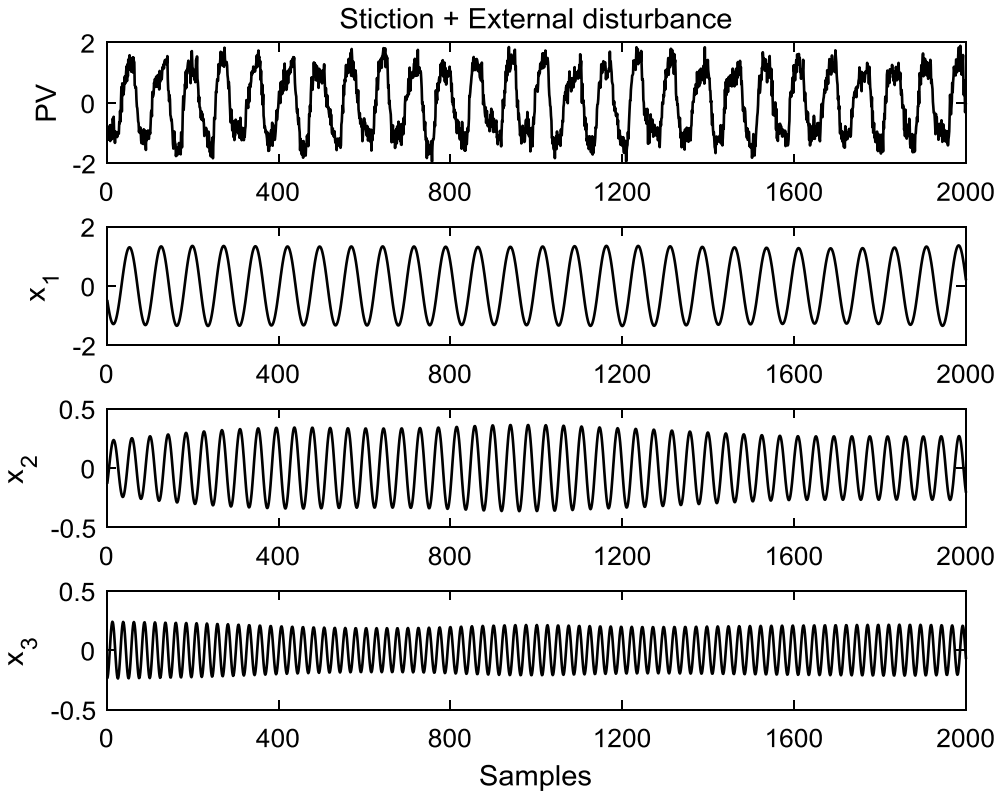

Fig. 25. Decomposition results of valve stiction with external disturbances.

Table 3
Detection results of the simulated SISO loop.

Case	Mode	ER_m	λ_m	c_m	SI_m	Oscillation?
Normal	x_1	1	–	–	–	No
	x_2	0.9694	–	–	–	
	x_3	0.9482	–	–	–	
Ext dist	x_1	1	1	0.9991	0.9948	Yes
Poor tuning	x_1	1	1	0.9814	0.8740	Yes
	x_2	0.2260	0.2810	0.9618	0.8716	
	x_3	0.1803	0.2035	0.9598	0.8636	
Ext dist + poor tuning	x_1	1	1	0.9785	0.8337	Yes
	x_2	0.3043	0.3743	0.9969	0.9954	
	x_3	0.2085	0.2837	0.9619	0.8700	
	x_4	0.1664	0.2063	0.9624	0.8704	
Stiction	x_1	1	1	0.9953	0.9686	Yes
	x_2	0.0823	0.1687	0.9958	0.9195	
Stiction+ ext dist	x_1	1	1	0.9951	0.9649	Yes
	x_2	0.1264	0.2369	0.9986	0.9359	
	x_3	0.0775	0.1559	0.9963	0.9102	

Table 4
Diagnosis results of the simulated SISO control loop.

Case	Mode	λ_m	IF_{mean}	IF_{min}	IF_{max}	Type	Result
Normal	–	–	–	–	–	–	Normal
Ext dist	x_1	1	0.0175	0.0175	0.0175	Ext dist	Ext dist
Poor tuning	x_1	1	0.0427	0.0415	0.0439	Poor tuning	Poor tuning
	x_2	0.2810	0.0468	0.0448	0.0488	Poor tuning	
	x_3	0.2035	0.0399	0.0378	0.0419	Poor tuning	
Ext dist+ Poor tuning	x_1	1	0.0427	0.0415	0.0439	Poor tuning	Ext dist+ Poor tuning
	x_2	0.3743	0.0175	0.0174	0.0176	Ext dist	
	x_3	0.2837	0.0468	0.0448	0.0489	Poor tuning	
	x_4	0.2063	0.0399	0.0379	0.0418	Poor tuning	
Stiction	x_1	1	0.0135	0.0133	0.0136	1st harmonic	Stiction
	x_2	0.1687	0.0404	0.0399	0.0410	3rd harmonic	
Stiction + ext dist	x_1	1	0.0135	0.0133	0.0136	1st harmonic	Stiction + ext dist
	x_2	0.2369	0.0239	0.0237	0.0241	Ext dist	
	x_3	0.1559	0.0404	0.0399	0.0409	3rd harmonic	

oscillations when they occur simultaneously, which cannot be achieved by most existing methods.

(v) Valve stiction

Fig. 24 displays the process variable and corresponding decomposition consequents for the dataset subject to valve stiction. Apparently, the loop output mainly consists of two harmonic components. Furthermore, based on the monitoring results of Tables 3 and 4, it can be observed that the oscillating modes x_1 and x_2 are characterized as the fundamental and the third order harmonics respectively by Algorithm 3, which means the proposed framework is able to capture the nonlinearity-induced oscillations correctly.

(vi) Valve stiction and external disturbance

The last case is the simulation in the abnormal condition with both valve stiction and external disturbances (with 0.0239 Hz). Its corresponding time trend and decomposition performance are given in Fig. 25, which indicates this process variable contains three components. The analysis indices in Tables 3 and 4 clearly manifest that this loop contains nonlinearity-induced oscillations plus linear external disturbances (with frequency approximating 0.0239 Hz). Still the proposed methodology can effectively differentiate multiple oscillations composed by both linear and nonlinear causes.

The aforementioned results demonstrate that the proposed approach is applicable for detecting and diagnosing different multiple oscillations. In the end, Table 5 records the corresponding running time of both FACMD and vanilla ACMD in a different case,[2] which indicates that the raised FACMD is indeed faster than the latter.

[2] FACMD and vanilla ACMD run ten times in the same conditions and their mean values are used to reduce errors.

Table 5
Running time of simulated SISO control loop (in seconds).

Method	Normal	Ext dist	Poor tuning	Ext dist + poor tuning	Stiction	Stiction + ext dist
FACMD	0.7719	0.0146	2.6268	0.8169	0.7938	0.5294
ACMD	2.9452	0.0158	5.9173	2.8027	2.6420	0.5998

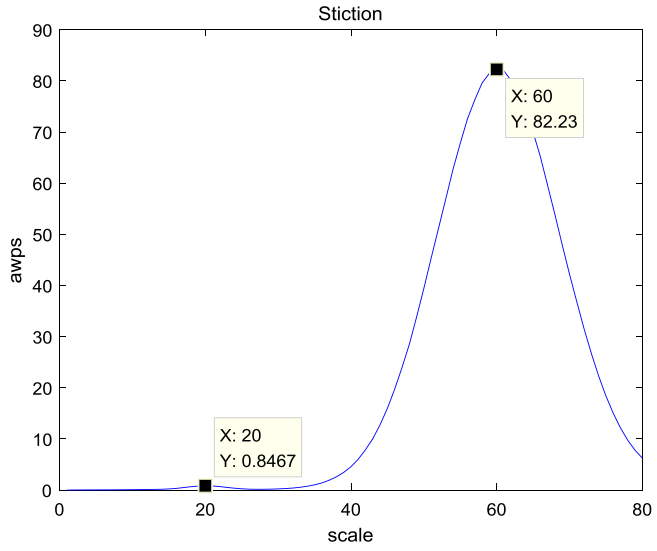

Fig. 26. AWPS of stiction.

Table 6
Detection and diagnosis results of the wavelet-based method (Naghoosi & Huang, 2017).

Case	Scale	Type	Result
Ext dist Poor tuning	46 19	Ext dist Poor tuning	Ext dist Poor tuning
Ext dist + poor tuning	47 19	Ext dist Poor tuning	Ext dist+ Poor tuning
Stiction	60 20	Nonlinear **Linear**	Nonlinear+ **Linear**
Stiction + ext dist	60 20	Nonlinear **Linear (not ext dist)**	Nonlinear+ **Linear (not ext dist)**

Table 7
Detection results of the industrial single loop control system.

Case	Mode	ER_m	λ_m	c_m	SI_m	Oscillation?
Normal	x_1 x_2 x_3	1 0.9511 0.9165	– – –	– – –	– – –	No
Ext dist	x_1	1	1	0.9979	0.9179	Yes
Poor tuning	x_1	1	1	0.9677	0.8884	Yes
Stiction	x_1 x_2	1 0.1853	1 0.2848	0.9809 0.9630	0.9140 0.8138	Yes

Recently the most important progresses in oscillation detection and diagnosis have been done by Naghoosi and Huang (2017), which was partly based on their previous work (Naghoosi & Huang, 2014b). To make fairer comparisons of the proposed methodology, the method of Naghoosi and Huang (2017) is also conducted for the above SISO control loop in various fault conditions. The corresponding results are listed in Table 6. It is observed that the wavelet-based method can detect and diagnose two types of linear oscillations and their combination correctly. However, it lacks the ability to deal with complex multiple linear/nonlinear oscillation. More specifically, (i) for the valve stiction case, the third order harmonic induced by nonlinearity is characterized as linear oscillations; (ii) for the valve stiction with the external disturbance case, in addition to the same problem described in (i), the wavelet-based method also misses the detection of external disturbances.

To explain the above issues, the method of Naghoosi and Huang (2017) is briefly reviewed here. In the wavelet decomposition based method, the oscillating scales are detected by the average of absolute

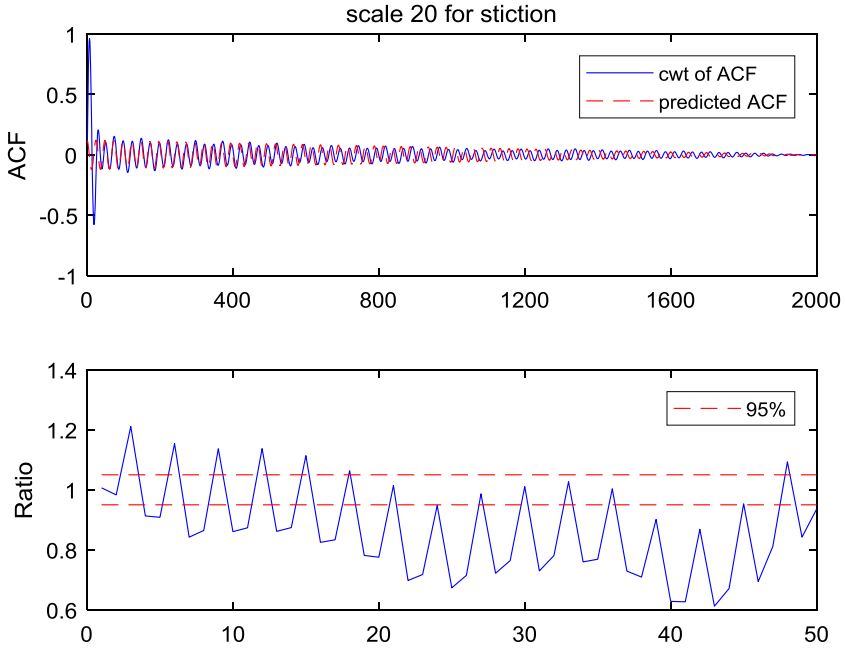

Fig. 27. Ratio curve for the stiction case at scale 20 . (For interpretation of the references to color in this figure legend, the reader is referred to the web version of this article.)

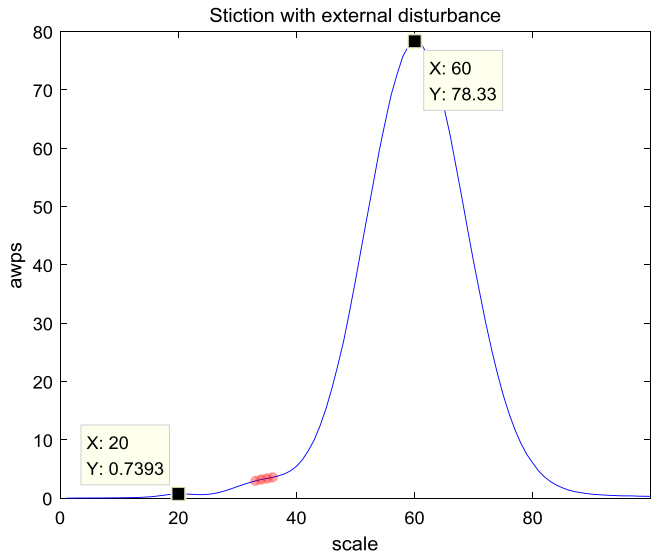

Fig. 28. AWPS of stiction with external disturbances . (For interpretation of the references to color in this figure legend, the reader is referred to the web version of this article.)

wavelet coefficients through time. The average of absolute wavelet coefficients is calculated as $awps_x(a) = \sum_{b=1}^{N} |w_x(b,a)|^2 / N$ and $w_x(b,a) = \frac{1}{\sqrt{a}} \int_{-\infty}^{+\infty} x(t) \psi^* \left(\frac{t-b}{a}\right) dt$, where b is the time point and a is the scale. Thus the local peaks in *awps* curve versus scale can correspond to the oscillation frequencies. To detect phase coupling in variables, wavelet-based bicoherence $wbic^2_{\max}(a_{osc}, a_2)$ is constructed. Using Chebyshev's inequality

$$P(|x-\mu| \geq d\sigma) \leq \frac{1}{d^2} \tag{23}$$

Table 8
Diagnosis results of the industrial single loop control system.

Case	Mode	λ_m	IF_{mean}	IF_{min}	IF_{max}	Type	Result
Normal	–	–	–	–	–	–	Normal
Ext dist	x_1	1	0.0005	0.0004	0.0006	Ext dist	Ext dist
Poor tuning	x_1	1	0.0178	0.0173	0.0184	Poor tuning	Poor tuning
Stiction	x_1	1	0.0008	0.0008	0.0008	1st harmonic	Stiction
	x_2	0.2848	0.0024	0.0023	0.0025	3rd harmonic	

where $\mu = \sum_{a_1 \neq a_{osc}} \sum_{a_2 \neq a_{osc}} wbic_x^2(a_1, a_2) / N$ and $x = wbic^2_{\max}(a_{osc}, a_2)$. If x is significantly different from μ, then the oscillation is induced by nonlinearity. To distinguish two types of linear oscillations, the ratio indicator is defined as

$$\frac{|w_{ACF}(b,a)|^2}{\left|p_r \frac{N-v}{N-v_r} \cos(2\pi\omega v)\right|^2} \tag{24}$$

If the ratio is significantly different from 1, it is concluded that the oscillation is regarded as poor controller tuning.

In this valve stiction case, the CWT coefficients of scale 20 correspond to the third order harmonic, which is induced by the nonlinearity rather than linear oscillations. The wavelet-bicoherence based hypothesis testing is based on measuring the relative magnitude of the oscillating scale with other scales; however, the third order harmonic has small energy (Fig. 26). Thus the nonlinear detection gets a false outcome. In addition, because of the limitations of the wavelet transform, the CWT coefficients of ACF at scale 20 are not a standard sinusoidal sequence, which leads to unsatisfactory linear testing (Fig. 27). In the valve stiction with the external disturbance case, in addition to the same problem discussed in the valve stiction case, external disturbances also cannot be detected. In Fig. 28, two distinct peaks are marked (nonlinearity-induced oscillations), but there actually should be a peak in the red area caused by the external harmonic.

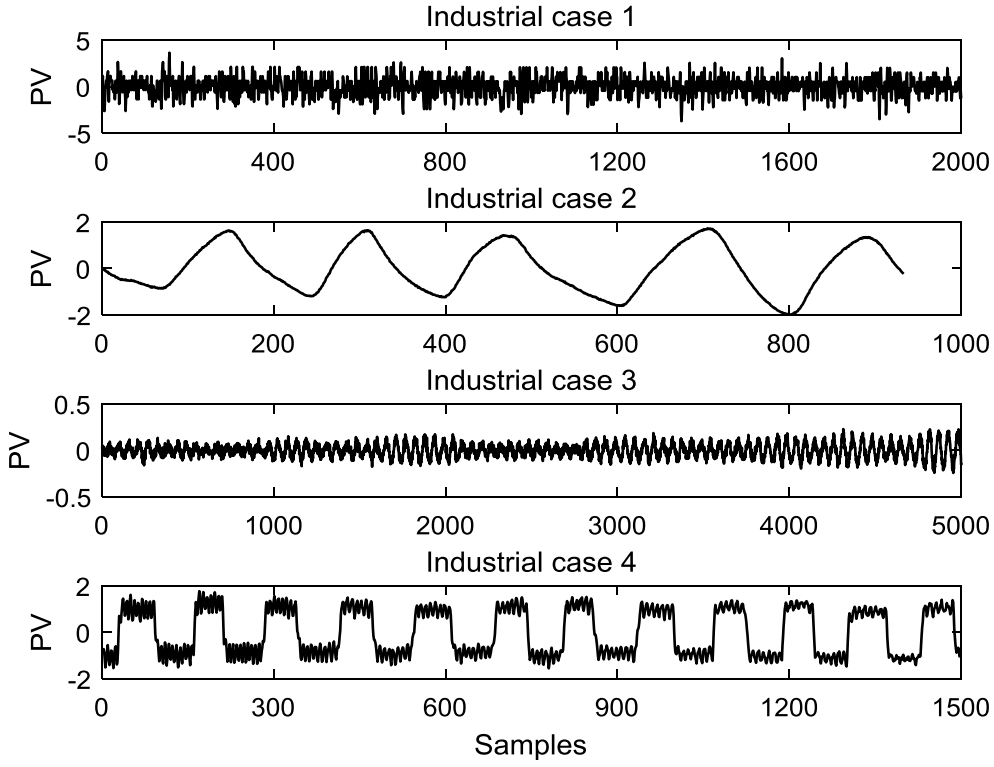

Fig. 29. Industrial data of single loop control system.

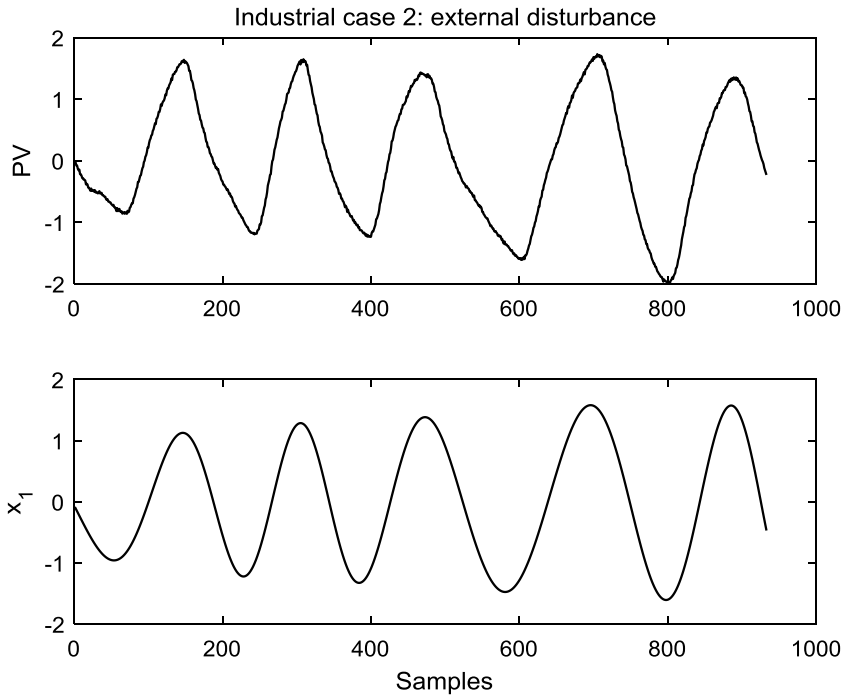

Fig. 30. Decomposition results of industrial case 2.

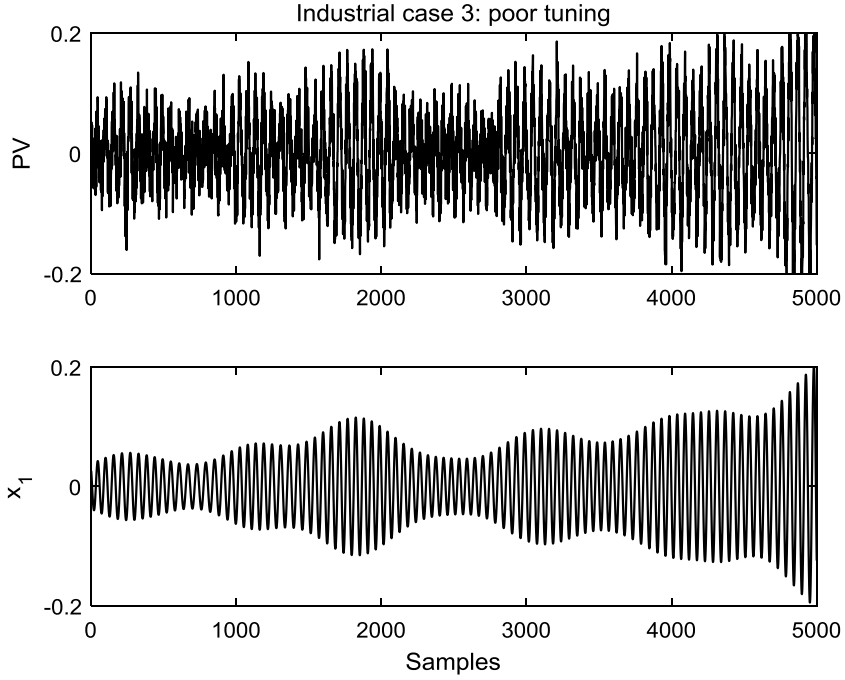

Fig. 31. Decomposition results of industrial case 3.

5.2. Industrial cases

Since the above simulations on the proposed methodology acts well, more widespread industrial applications can be expected. This subsection consists of two parts: (i) the proposed technique is used to detect and diagnose oscillations for an industrial single loop control system from the previous study (Jelali & Huang, 2009), and (ii) this method is used for the root cause analysis of plant-wide oscillations. In this industrial single loop control system, the proposed oscillation detection and diagnosis are applied to four representative cases shown in Fig. 29.

(i) Normal operation

The first industrial case is taken from a temperature control loop in a building field without oscillations, i.e., this loop is in the normal condition. The feature of interest in Table 7 is the energy ratio ER_m. Since ER_ms of the first three modes exceed the preset threshold, there is no oscillation in this loop.

(ii) External disturbances

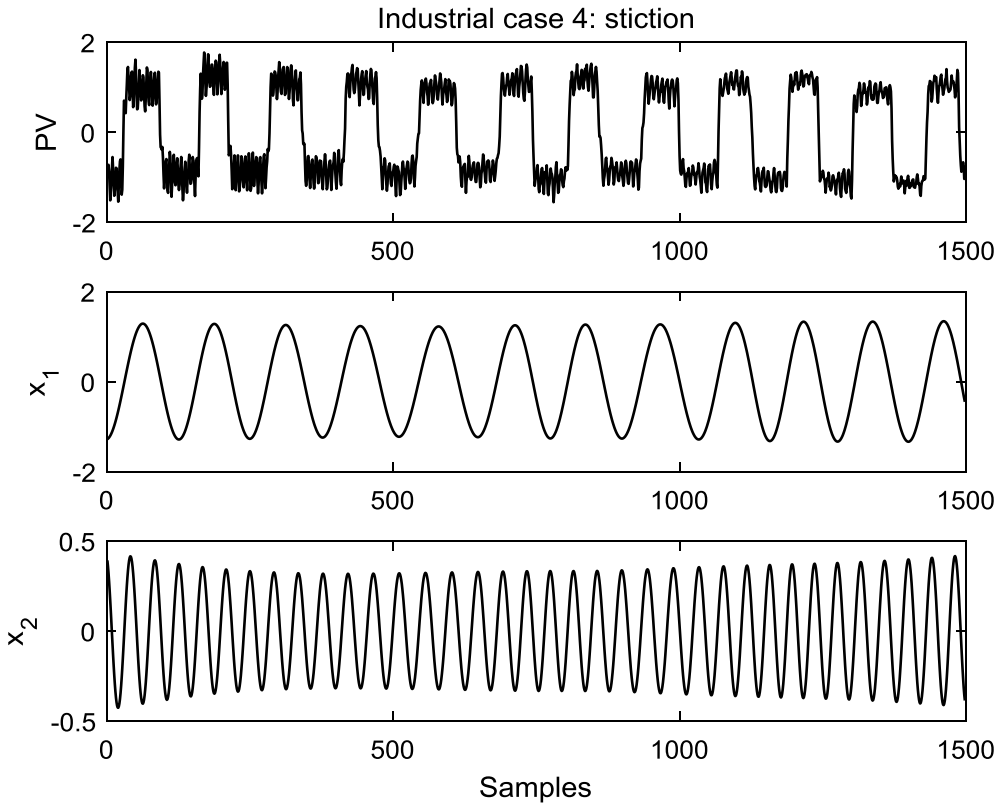

Fig. 32. Decomposition results of industrial case 4.

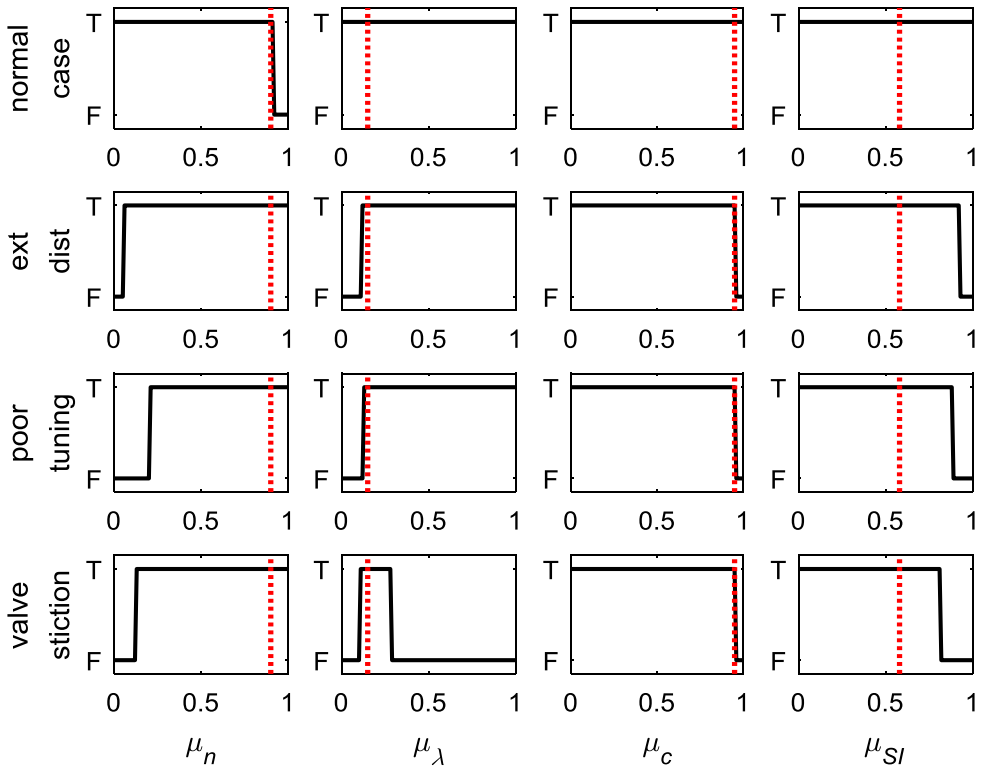

Fig. 33. Effects of changing parameters' threshold for industrial cases (normal operation, external disturbances, poor tuning, and valve stiction). T and F are short for TRUE and FALSE, respectively. The vertical red dotted lines show the default values . (For interpretation of the references to color in this figure legend, the reader is referred to the web version of this article.)

In this industrial case, the dataset is collected from a pressure control loop in a refinery plant, which is known to be subject to an external disturbance. Fig. 30 shows its decomposition results from FACMD, and the indicators in Tables 7 and 8 clearly reveal the presence

Table 9
Tuning reference for parameters.

Parameter	μ_n	μ_λ	μ_c	μ_{SI}
Reference	(0.20, 0.91)	(0.12,0.29)	(0,0.96)	(0,0.81)

Table 10
Detection and diagnosis results of plant-wide oscillations based on the proposed method.

Tag	Mode	λ_m	IF_{mean}	IF_{min}	IF_{max}	Harmonic	Results
2	x_1	1	0.0010	0.0010	0.0010	No	Linear
3	x_1 x_2	1 0.1779	0.0010 0.00034	0.0010 0.00031	0.0010 0.00036	No	Linear
4	x_1 x_2	1 0.2308	0.0010 0.00032	0.0010 0.00029	0.0010 0.00034	No	Linear
10	x_1	1	0.0010	0.0010	0.0010	No	Linear
11	x_1 x_2 x_3	1 0.5143 0.2674	0.0010 0.0002 0.0030	0.0010 0.00017 0.0030	0.0010 0.00023 0.0030	1st – 3rd	Nonlinear
13	x_1 x_2 x_{3+4+5}	1 0.3429 0.5583	0.0010 0.0020 0.0048	0.0010 0.0020 0.0047	0.0010 0.0020 0.0048	1st 2nd –	Nonlinear
19	x_1 x_2 x_3 x_4 x_5	1 0.5024 0.2494 0.2803 0.2246	0.0010 0.00021 0.0020 0.00035 0.0035	0.0010 0.00018 0.0020 0.00031 0.0035	0.0010 0.00024 0.0020 0.00039 0.0035	1st – 2nd – –	Nonlinear
20	x_1	1	0.0010	0.0010	0.0010	No	Linear
33	x_1 x_2	0.9793 0.2737	0.0010 0.0020	0.0010 0.0020	0.0010 0.0020	1st 2nd	Nonlinear
34	x_1 x_2 x_3	1 0.5014 0.3618	0.0010 0.0020 0.0050	0.0010 0.0020 0.0050	0.0010 0.0020 0.0051	1st 2nd 5th	Nonlinear

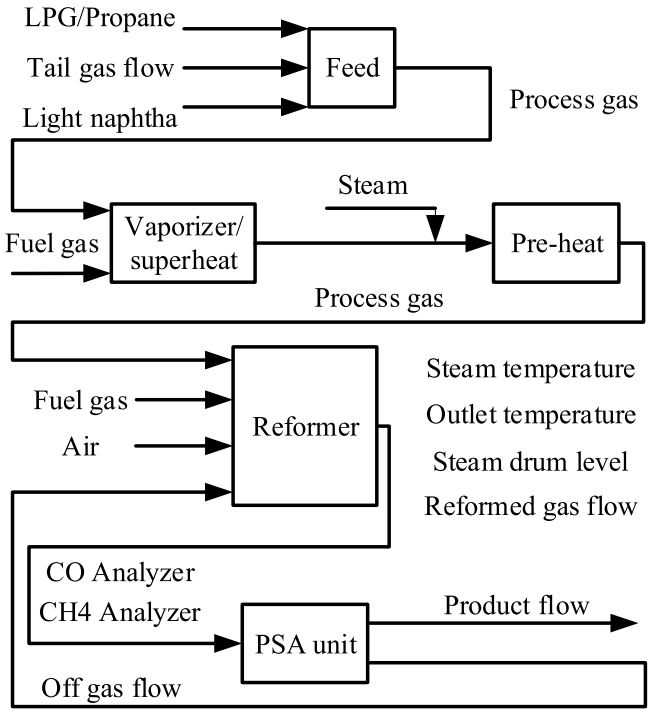

Fig. 34. Process schematic of plant-wide oscillations.

of an external harmonic disturbance with frequency approximating 0.0005 Hz.

Table 11
Detection and diagnosis results of plant-wide oscillations for wavelet-based and MEMD-based methods.

Tag	Wavelet-based		MEMD-based	
	Scale	Results	IMF	Results
2	13	**Nonlinear**	–	Linear
3	13 69	**Nonlinear** Linear	–	Linear
4	13 72	Linear Linear	–	Linear
10	13	Linear	–	Linear
11	11	Nonlinear	1 2 3	Nonlinear
13	13	Nonlinear	–	**Linear**
19	13 69	Linear Linear	–	Linear
20	13	**Nonlinear**	–	Linear
33	64	**Linear**	1 2	Nonlinear
34	13	Nonlinear	1 2 3	Nonlinear

(iii) Poor tuning

In this case, the detection and diagnosis are performed on the process variable data obtained from a level control loop. The decomposition outputs of the process variable are displayed in Fig. 31. It is known in advance that this loop is oscillating because of bad controller tuning. Based on the normal distribution testing in the oscillatory mode x_1, it can be concluded that the linear oscillations in this loop may be caused by poor controller tuning. The related specific data are provided in Tables 7 and 8.

(iv) Valve stiction

Fig. 32 exhibits the decomposition results of the proposed FACMD for the dataset with valve stiction, which is sampled from a flow control loop in a chemical process. The cases in Tables 7 and 8 present the detailed information on FACMD-based oscillation detection and diagnosis for this loop. From both tables, a third harmonic is detected. Thus it can be concluded that this loop suffers from valve stiction.

Remark. The effects of changing the thresholds on the energy ratio μ_n, the normalized correlation coefficient μ_λ, the consistency function μ_c, and the sparseness index μ_{SI} are analyzed for various industrial control loops. The corresponding results are given in Fig. 33. All these four thresholds vary from 0 to 1. It can be seen that the results are mostly stable with respect to these variations. The corresponding tuning references are provided in Table 9.

(v) Plant-wide oscillations

Although the oscillation is usually generated in one loop, it often propagates through the interconnected loops so that it causes plant-wide oscillations (Lang, Zhang, Xie, Horch and Su, 2018). Therefore, it is necessary to conduct the root cause analysis to find the root cause of plant-wide oscillations before the control problem is resolved via proper service and troubleshooting (Aftab, Hovd, & Sivalingam, 2018b).

To demonstrate the advantages of the proposed method in a real plant application, the comparative studies on an industrial plant-wide oscillation case are reported in this section. This industrial case is taken from a southeast Asian refinery. This dataset is widely used as a benchmark for plant-wide oscillation detection and diagnosis methods, e.g., Aftab et al. (2017, 2018a) and Thornhill (2005). Figs. 34 and 35

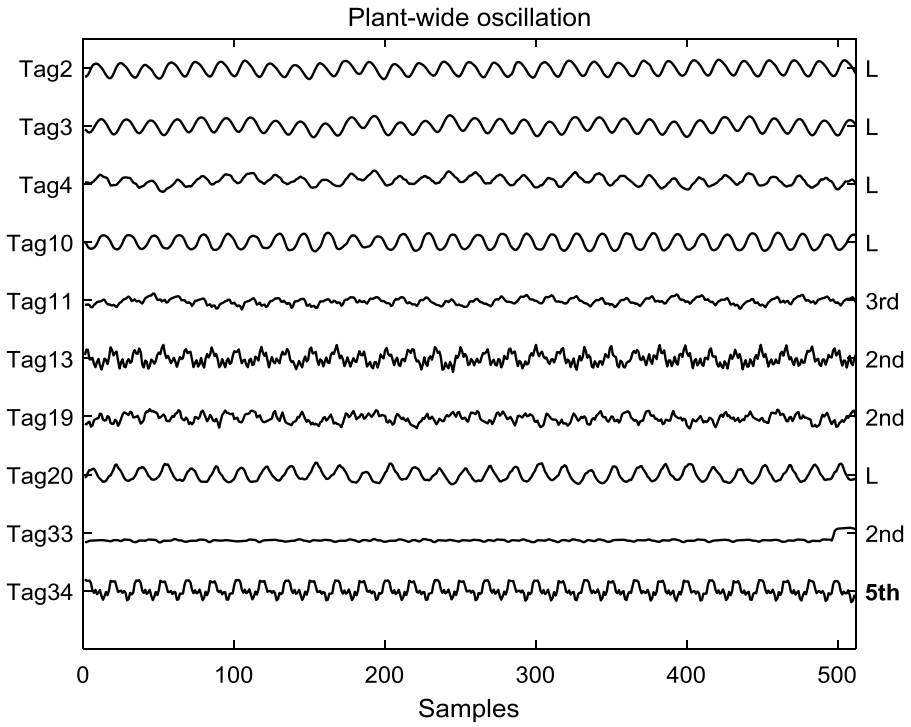

Fig. 35. Time trends from the industrial plant-wide oscillation case. The harmonic orders obtained by the proposed method are shown on the right-side.

show the process schematic and the corresponding time trends of a group of variables, respectively. The results about the detection and diagnosis results of plant-wide oscillations are given in Table 10. It is observed that the proposed method can take Tag 11, 13, 19, 33, and 34 as nonlinearity-induced oscillations. The harmonic orders detected by the proposed method are shown on the right side of Fig. 35. As the disturbance influences the other loops such as temperature, and composition, the waveform becomes more sinusoidal and more linear because low-pass plant dynamics removes the higher harmonics and destroys the phase coupling (Thornhill, Cox et al., 2003). It is found that Tag 34 contains the highest order, which can be regarded as the source of nonlinearities. Thus, Tag 34 is the most probable candidate for the root cause in the corresponding loop. Also, this conclusion is in agreement with previous studies (Thornhill, 2005).

Their detection and diagnosis results of the other methods, such as wavelet-based (Naghoosi & Huang, 2017) and MEMD-based (Aftab et al., 2017) algorithms, are listed in Table 11. In this table, the bold labels indicate misjudgments. The wavelet-based method can identify most nonlinear oscillations, but it is more likely to misjudge linear oscillations as nonlinear oscillations, such as Tag 2, 3, and 20. The performance of the MEMD-based method seems to perform better than that of the wavelet-based one. There is one misdiagnosed case in Tag 13 as the second harmonic is not regular according to Aftab et al. (2017).

Remark. Over-decomposition is a common issue in various signal decomposition methods (Dragomiretskiy & Zosso, 2013). Summing different modes with similar frequencies is a universal and effective way to deal with this issue (Lang, Zhang et al., 2018; ur Rehman, Park, Huang, & Mandic, 2013; Wu & Huang, 2009). In the plant-wide oscillation case, it is found that only Tag 13 suffers from over-decomposition, which means this issue is a non-frequent problem of the proposed method. Fig. 36 shows the instantaneous frequencies of five modes contained in Tag 13. In this figure, x_3, x_4, and x_5 have similar frequency information. It is reasonable to reduce the number of modes by the summation of x_3, x_4, and x_5. Even though more modes are extracted, the oscillation behaviors are similar. Therefore, the detection and diagnosis results are still correct.

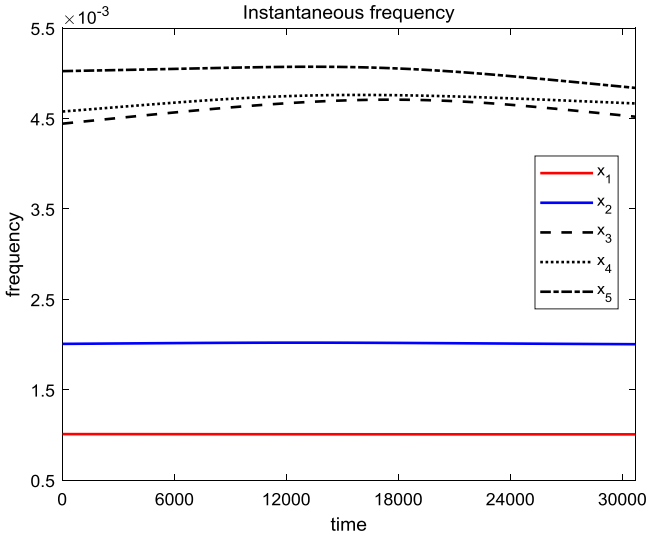

Fig. 36. The instantaneous frequencies of Tag 13 . (For interpretation of the references to color in this figure legend, the reader is referred to the web version of this article.)

6. Conclusions

This paper proposed the FACMD algorithm at first. Then the methodology of detecting and diagnosing oscillations is devised based on FACMD. It is able to identify and distinguish oscillations into three common types, i.e. nonlinearity, external harmonic disturbance and poor controller tuning. In addition to dealing with various single/multiple oscillations in the SISO loop, it is capable of contributing to analyzing the root cause for plant-wide oscillations. The proposed methodology has better detection and diagnosis accuracy and a higher level of automation than the existing methods, especially in processing complex multiple oscillations. At last, a series of simulations and industrial cases are provided to verify its effectiveness and advantages.

The favorable outcomes in the testing cases indicate that the proposed technique can be readily implemented in the industrial environment. In the future, some issues about this method will still be considered, for example, it cannot distinguish two types of linear oscillations when the data length is too short.

Declaration of competing interest

The authors declare that they have no known competing financial interests or personal relationships that could have appeared to influence the work reported in this paper.

Acknowledgments

The authors would like to thank the sponsors from National Key R&D Program of China (No. 2018YFB1701102), Natural Science Foundation of Zhejiang, China under grand No. LR17F030002, Science Fund for Creative Research Groups of the National Natural Science Foundation of China (Grant No.61621002), and Ministry of Science and Technology, Taiwan, R.O.C. (MOST 106-2221-E-033-060-MY3) for their financial support.

References

Aftab, M. F., Hovd, M., Huang, N. E., & Sivalingam, S. (2016). An adaptive non-linearity detection algorithm for process control loops. *IFAC-PapersOnLine*, *49*, 1020–1025.

Aftab, M. F., Hovd, M., & Sivalingam, S. (2017). Detecting non-linearity induced oscillations via the dyadic filter bank property of multivariate empirical mode decomposition. *Journal of Process Control*, *60*, 68–81.

Aftab, M. F., Hovd, M., & Sivalingam, S. (2018a). Improved oscillation detection via noise-assisted data analysis. *Control Engineering Practice*, *81*, 162–171.

Aftab, M. F., Hovd, M., & Sivalingam, S. (2018b). Plant-wide oscillation detection using multivariate empirical mode decomposition. *Computers & Chemical Engineering*, *117*, 320–330.

Babji, S., Nallasivam, U., & Rengaswamy, R. (2012). Root cause analysis of linear closed-loop oscillatory chemical process systems. *Industrial & Engineering Chemistry Research*, *51*, 13712–13731.

Chen, S., Dong, X., Peng, Z., Zhang, W., & Meng, G. (2017). Nonlinear chirp mode decomposition: A variational method. *IEEE Transactions on Signal Processing*, *65*, 6024–6037.

Chen, S., Yang, Y., Peng, Z., Dong, X., Zhang, W., & Meng, G. (2019). Adaptive chirp mode pursuit: Algorithm and applications. *Mechanical Systems and Signal Processing*, *116*, 566–584.

Chen, S., Yang, Y., Peng, Z., Wang, S., Zhang, W., & Chen, X. (2019). Detection of rub-impact fault for rotor-stator systems: A novel method based on adaptive chirp mode decomposition. *Journal of Sound and Vibration*, *440*, 83–99.

Choudhury, A. A. S., Shah, S. L., & Thornhill, N. F. (2008). *Diagnosis of process nonlinearities and valve stiction: Data driven approaches*. Springer Science & Business Media.

Choudhury, M. S., Thornhill, N. F., & Shah, S. L. (2005). Modelling valve stiction. *Control Engineering Practice*, *13*, 641–658.

Dewa, G. R., Wardana, A. N., & Hawibowo, S. (2018). Linear oscillation diagnosis of process variable in control loop based on variational mode decomposition. In *2018 4th international conference on science and technology* (pp. 1–5). IEEE.

Dragomiretskiy, K., & Zosso, D. (2013). Variational mode decomposition. *IEEE Transactions on Signal Processing*, *62*, 531–544.

Forsman, K., & Stattin, A. (1999). A new criterion for detecting oscillations in control loops. In *1999 European control conference* (pp. 2313–2316). IEEE.

Frei, M. G., & Osorio, I. (2006). Intrinsic time-scale decomposition: time–frequency–energy analysis and real-time filtering of non-stationary signals. *Proceedings of the Royal Society A: Mathematical, Physical and Engineering Sciences*, *463*, 321–342.

Guo, Z., Xie, L., Ye, T., & Horch, A. (2014). Online detection of time-variant oscillations based on improved ITD. *Control Engineering Practice*, *32*, 64–72.

Hägglund, T. (1995). A control-loop performance monitor. *Control Engineering Practice*, *3*, 1543–1551.

Huang, N. E., Shen, Z., Long, S. R., Wu, M. C., Shih, H. H., Zheng, Q., et al. (1998). The empirical mode decomposition and the Hilbert spectrum for nonlinear and non-stationary time series analysis. *Proceedings of the Royal Society of London. Series A: Mathematical, Physical and Engineering Sciences*, *454*, 903–995.

Iwashita, Y. (1992). Method of detecting oscillation of a servo system and automatically adjusting speed loop gain thereof. Google Patents.

Jelali, M., & Huang, B. (2009). *Detection and diagnosis of stiction in control loops: State of the art and advanced methods*. Springer Science & Business Media.

Karra, S., & Karim, M. N. (2009). Comprehensive methodology for detection and diagnosis of oscillatory control loops. *Control Engineering Practice*, *17*, 939–956.

Lang, X., Lu, S., Xie, L., Zakharov, A., Zhong, D., & Jämsä-Jounela, S.-L. (2018). Bihocerence based industrial control loop nonlinearity detection and diagnosis in short nonstationary time series. *Journal of Process Control*, *63*, 15–28.

Lang, X., Zhang, Z., Xie, L., Horch, A., & Su, H. (2018). Time-frequency analysis of plant-wide oscillations using multivariate intrinsic time-scale decomposition. *Industrial and Engineering Chemistry Research*, *57*, 954–966.

Lang, X., Zheng, Q., Zhang, Z., Lu, S., Xie, L., Horch, A., et al. (2018). Fast multivariate empirical mode decomposition. *IEEE Access*, *6*, 65521–65538.

Li, X., Wang, J., Huang, B., & Lu, S. (2010). The DCT-based oscillation detection method for a single time series. *Journal of Process Control*, *20*, 609–617.

Miao, T., & Seborg, D. E. (1999). Automatic detection of excessively oscillatory feedback control loops. In *Proceedings of the 1999 IEEE international conference on control applications (Cat No 99CH36328)* (pp. 359–364). IEEE.

Naghoosi, E., & Huang, B. (2014a). Automatic detection and frequency estimation of oscillatory variables in the presence of multiple oscillations. *Industrial and Engineering Chemistry Research*, *53*, 9427–9438.

Naghoosi, E., & Huang, B. (2014b). Diagnosis of oscillations between controller tuning and harmonic external disturbances. *IEEE Transactions on Control Systems Technology*, *23*, 1283–1293.

Naghoosi, E., & Huang, B. (2017). Wavelet transform based methodology for detection and characterization of multiple oscillations in nonstationary variables. *Industrial and Engineering Chemistry Research*, *56*, 2083–2093.

Smith, J. S. (2005). The local mean decomposition and its application to EEG perception data. *Journal of the Royal Society Interface*, *2*, 443–454.

Srinivasan, B., & Rengaswamy, R. (2012). Automatic oscillation detection and characterization in closed-loop systems. *Control Engineering Practice*, *20*, 733–746.

Srinivasan, R., Rengaswamy, R., & Miller, R. (2007). A modified empirical mode decomposition (EMD) process for oscillation characterization in control loops. *Control Engineering Practice*, *15*, 1135–1148.

Thornhill, N. F. (2005). Finding the source of nonlinearity in a process with plant-wide oscillation. *IEEE Transactions on Control Systems Technology*, *13*, 434–443.

Thornhill, N. F., Cox, J. W., & Paulonis, M. A. (2003). Diagnosis of plant-wide oscillation through data-driven analysis and process understanding. *Control Engineering Practice*, *11*, 1481–1490.

Thornhill, N. F., Huang, B., & Zhang, H. (2003). Detection of multiple oscillations in control loops. *Journal of Process Control*, *13*, 91–100.

Ullah, M. F., Das, L., Parmar, S., Rengaswamy, R., & Srinivasan, B. (2019). On developing a framework for detection of oscillations in data. *ISA Transactions*.

ur Rehman, N., Park, C., Huang, N. E., & Mandic, D. P. (2013). EMD via MEMD: multivariate noise-aided computation of standard EMD. *Advances in Adaptive Data Analysis*, *5*, 1350007.

Wang, Y., & Markert, R. (2016). Filter bank property of variational mode decomposition and its applications. *Signal Processing*, *120*, 509–521.

Wardana, A. N. (2015). A method for detecting the oscillation in control loops based on variational mode decomposition. In *2015 international conference on computer, control, informatics and its applications* (pp. 181–186). IEEE.

Wu, Z., & Huang, N. E. (2009). Ensemble empirical mode decomposition: a noise-assisted data analysis method. *Advances in Adaptive Data Analysis*, *1*, 1–41.

Xie, L., Lang, X., Chen, J., Horch, A., & Su, H. (2016). Time-varying oscillation detector based on improved LMD and robust Lempel–Ziv complexity. *Control Engineering Practice*, *51*, 48–57.